AD_____

Award Number: DAMD17-97-1-7339

TITLE: Dissection of the Pathogenesis of Neurofibromatosis Type 1-Associated Myeloid Leukemia

PRINCIPAL INVESTIGATOR: Camilynn I. Brannan, Ph.D.

CONTRACTING ORGANIZATION: University of Florida
Gainesville, Florida 32611-2037

REPORT DATE: October 2001

TYPE OF REPORT: Final

PREPARED FOR: U.S. Army Medical Research and Materiel Command
Fort Detrick, Maryland 21702-5012

REPORT DOCUMENTATION PAGE

Form Approved
OMB No. 074-0188

1. AGENCY USE ONLY (Leave blank)	2. REPORT DATE	3. REPORT TYPE AND DATES COVERED
	October 2001	Final (19 Sep 97 - 18 Sep 01)

4. TITLE AND SUBTITLE
Dissection of the Pathogenesis of Neurofibromatosis Type 1-Associated Myeloid Leukemia

5. FUNDING NUMBERS
DAMD17-97-1-7339

6. AUTHOR(S)
Camilynn I. Brannan, Ph.D.

7. PERFORMING ORGANIZATION NAME(S) AND ADDRESS(ES)
University of Florida
Gainesville, Florida 32611-2037

E-Mail: brannan@mgm.ufl.edu

8. PERFORMING ORGANIZATION REPORT NUMBER

9. SPONSORING / MONITORING AGENCY NAME(S) AND ADDRESS(ES)
U.S. Army Medical Research and Materiel Command
Fort Detrick, Maryland 21702-5012

10. SPONSORING / MONITORING AGENCY REPORT NUMBER

11. SUPPLEMENTARY NOTES
Report contains color

12a. DISTRIBUTION / AVAILABILITY STATEMENT
Approved for Public Release; Distribution Unlimited

12b. DISTRIBUTION CODE

13. ABSTRACT ***(Maximum 200 Words)***

Although most of the tumors associated with neurofibromatosis type 1 (NF1) are benign in nature, malignant transformation of a subset of NF1 tumors is a serious complication, often leading to the death of the patient. This is true for NF1-associated juvenile myelomonocytic leukemia (JMML), known to progress into acute myeloid leukemia (AML). Previously,we have shown that loss of *Nf1* in the hematopoetic lineage results in JMML. The goal of this grant is to identify the genetic events which lead to the transformation and leukemic progression of NF1-associated JMML using a mouse model. This model system takes advantage of transgenic mice that harbor one mutant allele of the *Nf1* gene, but require further mutations for transformation. We have backcrossed this mutant *Nf1* allele for three generations to a strain of mouse that expresses a murine leukemia virus (MuLV). In this system, the MuLV acts as a mutagen to activate cooperating cellular proto-oncogenes or inactivate tumor suppressor genes, resulting in accelerated tumor development. So far, by cloning sites of somatic MuLV integration from tumor DNAs obtained from these backcrossed mice, we have identified three loci that appear to cooperate with the loss of *Nf1* to cause to AML.

14. SUBJECT TERMS
Neurofibromatosis, tumor progression, myeloid leukemia

15. NUMBER OF PAGES
26

16. PRICE CODE

17. SECURITY CLASSIFICATION OF REPORT	18. SECURITY CLASSIFICATION OF THIS PAGE	19. SECURITY CLASSIFICATION OF ABSTRACT	20. LIMITATION OF ABSTRACT
Unclassified	Unclassified	Unclassified	Unlimited

Table of Contents

Introduction

Children with neurofibromatosis type 1 (NF1) have a markedly increased risk for juvenile myelomonocytic leukemia (JMML). JMML has a poor prognosis, with either progression to acute myeloid leukemia or death from bleeding or infection. Using a mouse model of NF1, we demonstrated that the lack of the *Nf1* gene in hematopoietic cells is sufficient to cause chronic myeloid leukemia, but not acute myeloid leukemia, indicating that additional genetic events are responsible for the progression from chronic to acute disease. The goal of this proposal is to identify and isolate genes involved in this leukemic progression. Toward this end, we are using a mouse model system which takes advantage of mice that harbor one mutant allele of the *Nf1* gene but require further mutation for transformation to neoplasia. The general strategy is to breed the mutant *Nf1* allele onto a strain of mouse that expresses murine leukemia virus (MuLV) and exhibits a high incidence of acute myeloid leukemia. In this system, the MuLV acts as a somatic mutagen to activate cooperating cellular proto-oncogenes or inactivate tumor suppressor genes, resulting in accelerated tumor development. Since MuLVs activate proto-oncogenes by integrating nearby or inactivate tumor suppressor genes by integrating within the gene, the affected genes can thus be identified and cloned using these somatically acquired viruses as signposts. The most promising loci are the ones that have sustained proviral insertion in tumors of multiple mice. The identification of a so-called "common site of viral integration" strongly indicates that the region harbors a gene, that when mutated by the virus, is directly involved in the development of myeloid leukemia. To date, we have identified three common sites of viral integration and are in the process of identifying and/or characterizing the gene affected by each site.

Technical Objective 1: Identify regions of the genome that cooperate with loss of *Nf1* in myeloid leukemia to cause tumor progression. Our objective was to produce a panel of tumors derived from heterozygous N3 generation BXH-2 $Nf1^{Fcr}$/+ mice. This panel was then to be used to identify new common sites of viral integration. This objective was divided into six tasks.

Task 1: *Produce F1, then N2, followed by N3 BXH-2 $Nf1^{Fcr}$/+ mice.*
Our initial strategy was to complete production of each generation before going onto the next. However, in practice, this strategy did not work, mainly because the parental BXH-2 strain to which we backcrossed had small litters. Therefore, we staggered the breeding to keep in line with the BXH-2 production.

Task 2: *Age N3 generation BXH-2 $Nf1^{Fcr}$/+ mice.*
At the time of the 1999 annual report, we had 33 animals in aging and were confident that the project would satisfy our goal of isolating lymph node tumors from approximately 100 independent animals by the end of the budget period. However, in February 2000, all of the 33 mice in aging died due to a bacterial infection that spread through the mouse room. Therefore, we reimported our mouse stocks and have repeated the required three generations of breeding. We currently have 42 N3 mice in aging and expect to reach the 100 tumor goal by February 2002.

Task 3: *Collect moribund animals. Process tumor sample. Assess the status of the wild-type Nf1 allele; determine the number of somatically acquired viral integrations; phenotypic analysis.*
To date, we have collected and characterized tumors from 66 N3 BXH-2 $Nf1^{Fcr}$/+ tumors. Each of these tumors have been examined for loss of the remaining normal *Nf1* allele and the number of somatically acquired viral integrations. We have determined that 59 of these tumors contain either LOH for *Nf1* or a viral integration at *Evi-2*. Therefore, by backcrossing the $Nf1^{Fcr}$ mutation onto the BXH-2 background, we have increased the incidence of tumors involving the *Nf1*-pathway from the 10-15% observed in the parental BXH-2 strain to an incidence of 89%. Finally, we determined the number of somatic viral integrations for each tumor. The tumors have a mean number of 3 such viral integrations.

Tasks 4, 5 and 6: *Clone somatically acquired proviruses from tumor samples which harbor defects in the wild-type Nf1 allele and have only one or two somatic proviral insertions. Prepare genomic flanking probes to screen tumor panel. Screen with probes to identify common sites of viral integration. Use probes that recognize common sites of viral insertion to isolate cosmid DNA. Begin studies to identify and characterize affected gene.*
The Southern blots have been prepared using all the available tumor samples. Using these Southern blots, we have been able to identify three common sites of viral integration: *Epi1*, affected in 48% of the

tumors; *Epi2* affected in 3% of the tumors; and *Epi3* affected in 3% of the tumors. For report on each site, please refer to Technical Objective 2.

Technical Objective 2: Characterize loci containing a gene involved in tumor progression. Our objective has been to identify the genes affected by the *Epi1, Epi2* and *Epi3* common sites of viral integration. The progress for each locus will be reported.

***Epi1:* Tasks 1, 2 and 3:** *Exon trap cosmid isolated with flanking probe. Identify gene. Isolate cDNA clones. Determine the genomic structure and normal expression pattern of the gene. Determine orientation of the gene relative to the viral integrations. Establish if virus activates or eliminates gene expression.* The lone somatic viral integration site was cloned from tumor #355. A genomic fragment flanking the site of viral integration was used to screen the tumor panel and rearrangements were detected in several independent tumors. Initially, we named this common site *Epi1* (Ecotropic proviral integration site 1). The genomic flanking probe was then used to genetically map the common site of viral integration to chromosome 10, cosegregating with the c-*myb* gene. Using a c-*myb* cDNA probe, we determined that both the common site and the c-*myb* gene were contained on a BAC clone (a cosmid proved to be too small so we moved to a BAC library), indicating that the two loci were physically linked. We have isolated multiple probes downstream of the c-*myb* gene and identified a total to 29 tumors (48% of the panel) with viral integrations downstream of c-*myb*.

Most previously reported viral integrations proven to affect c-*myb* have occurred within the c-*myb* gene and result in overexpression of a truncated oncogenic product (Wolff, 1996). However, our working hypothesis is that viral integrations at *Epi1* do affect the c-*myb* gene. To determine how 3' viral insertions affect c-*myb* expression, we examined the orientation of the virus in 13 of the tumors in which we knew contained full length virus (and hence were able to orient). We found that in all 13 cases, the virus had integrated in the same transcriptional orientation as the c-*myb* gene. These data are consistent with gene activation occuring by an enhancer insertion mechanism. With this in mind, we assayed the level of c-*myb* expression in the tumors using a Northern blot containing total RNA isolated from several of tumors with and one without a viral integration near c-*myb*. We found that c-*myb* expression levels do not appear to be increased in tumors containing a viral insertion near the c-*myb* locus relative to those tumors lacking such a viral insertion. Therefore, we speculate that the virus serves to prevent transcriptional downregulation of c-*myb*, a process known to be required for terminal differentiation of the myeloid (reviewed in (Oh, 1999)). We have published our results in the enclosed *Journal of Viriology* manuscript.

***Epi2:* Tasks 1, 2 and 3:** *Exon trap cosmid isolated with flanking probe. Identify gene. Isolate cDNA clones. Determine the genomic structure and normal expression pattern of the gene. Determine orientation of the gene relative to the viral integrations. Establish if virus activates or eliminates gene expression.* As the exon trap approach did not work, we sought alternate means to identify the affected gene. In collaboration with the Copeland and Jenkins laboratory, *Epi2* was mapped to a region of mouse chromosome 17 syntenic to human chromosome 6p21 and cosegregated with two known genes. To determine if either genetically linked gene was physically linked to our common site, we screened the Research Genetics BAC library with the common site probe and identified two BAC clones. We found that neither gene was on the BAC clones and thus eliminated them as candidate genes. To identify to the gene affected by these viral integrations, we sequenced 2.7 kb of the genomic DNA adjacent to the site of viral insertion. In September 2001, we found this flanking DNA to be homologous to a newly deposited murine cDNA sequence for the murine mitochondrial S18a subunit. Thus, we have identified the gene that is disrupted by the *Epi2* viral integrations. Northern blot analysis has shown that *Epi2* is expressed in heart, liver, and is also detectable in testis (Fig. 1A). We have isolated full length cDNA clones for *Epi2*, confirming the identity of this gene.

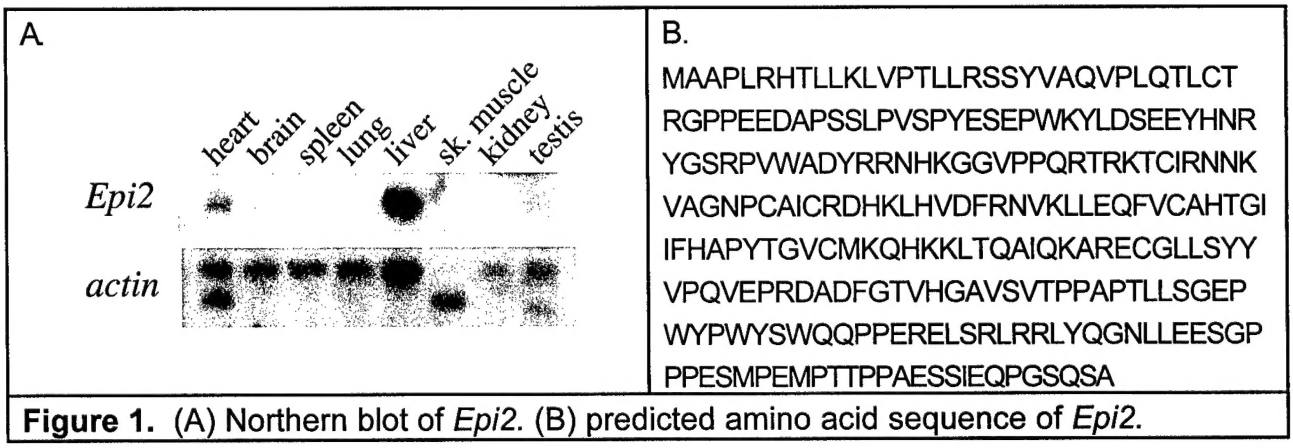

Figure 1. (A) Northern blot of *Epi2*. (B) predicted amino acid sequence of *Epi2*.

We are currently seeking to determine if the viral intergrations activate or in inactivate this gene. Our data indicates that viral integration has occurred in the first intron in the same transcriptional orientation as the gene in both tumors. This suggests that the "*Epi2*" gene has been mutated by one of two protein truncation mechanisms: either by promoter insertion, resulting in a 5' protein truncation (Fig. 2A), or via premature transcriptional termination, resulting in a 3' protein truncation (Fig. 2B). To determine which of these two possible mechanisms are at work, we propose to look for a fusion transcript between *Epi2* and viral elements. Our current hypothesis is that the viral integrations disrupt transcription of this gene, resulting in happloinsufficiency.

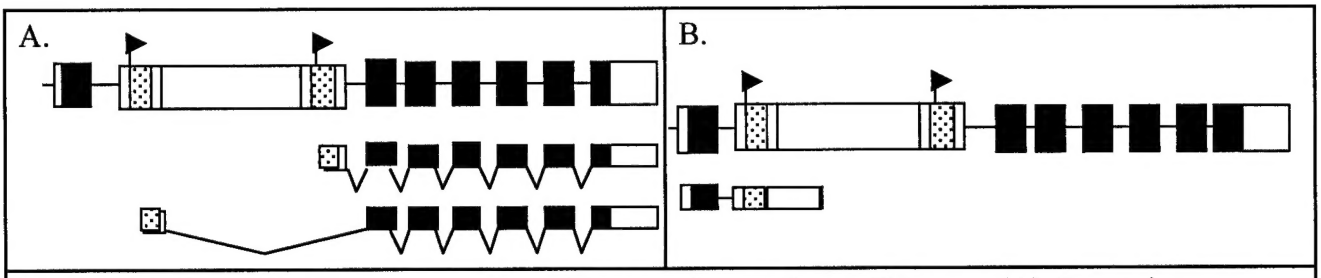

Figure 2. Potential consequences of viral integration at the *Epi2* locus. (A) 5' protein truncation mechanism caused by transcription initiation from the 3' LTR or the 5' LTR, followed by transcriptional termination at the normal position. (B) 3' protein truncation mechanism caused by transcription initiation at the normal promoter followed by premature transcriptional termination in the 5' viral long terminal repeat (LTR)

***Epi3:* Tasks 1 and 2:** *Exon trap cosmid isolated with flanking probe. Identify gene. Isolate cDNA clones. Determine the genomic structure and normal expression pattern of the gene. Determine orientation of the gene relative to the viral integrations. Epi3* has been mapped to a region of mouse chromosome 4 that is syntenic to human chromosome 1p35-p31. During the mapping, it was determined that there was a related sequence, dubbed *Epi3-rs*, that was found to map to mouse chromosome 17 in a region syntenic to human chromosome 6q25-q27. We have determined that *Epi3* is expressed in the heart, liver , kidney and testis and encodes a 1.4 kb mRNA (Fig. 3A). Based on comparing cDNA sequences to genomic sequences, we believe that there are 3 exons capable of encoding a 307 amino acid protein (Fig. 3B). So far, we have found no strong homology matches in the database to give us a clue as to the function of this protein. Future research will be required to investigate the role of this gene in leukemia.

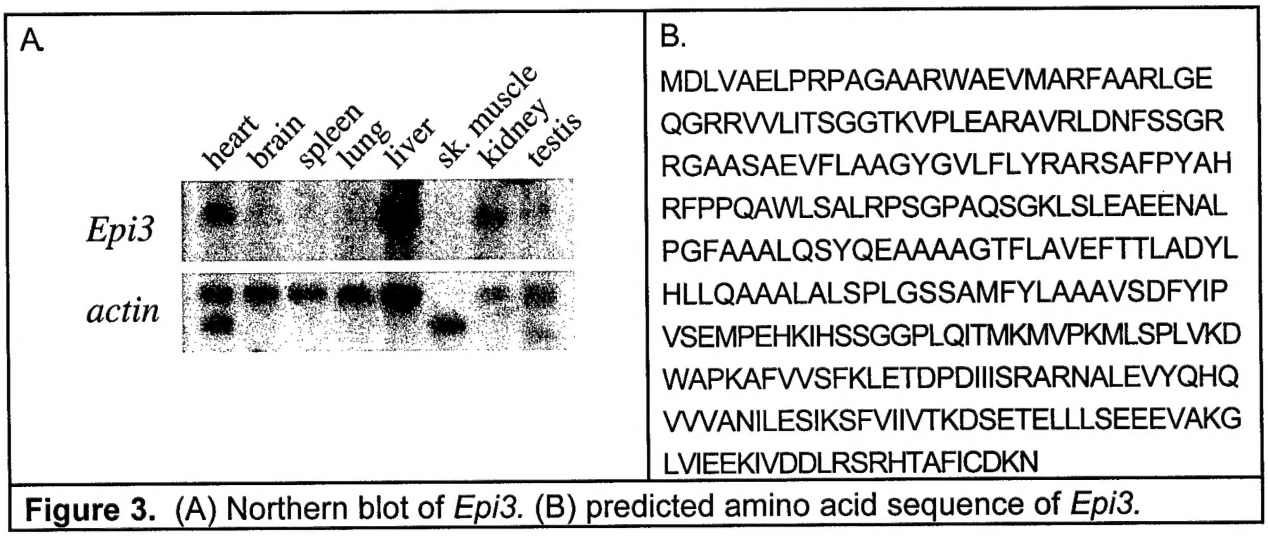

Figure 3. (A) Northern blot of *Epi3*. (B) predicted amino acid sequence of *Epi3*.

Task 4: *Create knock-out construct for the isolated gene. Transfect and isolate ES clones that have undergone gene targeting. Inject ES clones into blastocysts to generate a line of mice that harbor the gene knock-out mutation in their germline. Study phenotype of mice homozygous for the mutation.*

Due to the delay in identifying the *Epi2* gene and the fact that there is already a pre-existing knock-out of the c-*myb* gene, we have instead created a novel mutation in the *Nf1* gene (see below). The *NF1* gene encodes neurofibromin, a large protein with multiple isoforms produced as a result of alternative splicing. One of these alternatively spliced exons is exon 23a which encodes 21 amino acids (aa) in the middle of the GAP-related domain. Type I neurofibromin has been defined as not the isoform lacking these additional 21 aa whereas the type II isoform contains them. Others have shown that type II neurofibromin has a 10-fold decrease in GTPase activating protein (GAP) activity, but has a greater affinity for *Ras* (Andersen et al., 1993). In additional, some have suggested that the ratio of type I to type II isoforms may reflect and/or influence differentiation status (Gutmann et al., 1993; Nishi et al., 1991). Therefore, to investigate the function of type II isoform of neurofibromin, we generated mice that specifically lack exon 23a (*Nf123a*$^{-/-}$). So far, using intercrossing of heterozygous mice, we have been able to show that mice homozygous for this mutation are viable and lack type II isoform in brain tissue. In the past year, we have characterized the mutant mice at the histological and behavioral level and published our results in the enclosed *Nature Genetics* manuscript.

Key Research Accomplishments

- Production of a panel of murine acute myeloid leukemia tumors that lack the wild type *Nf1* gene product
- Identification of a locus, *Epi1*, which appears to cooperate with the loss of *Nf1* to cause acute myeloid leukemia (affected in 48% of the tumors in panel)
- Identification of a gene, *Epi2*, which appears to cooperate with the loss of *Nf1* to cause acute myeloid leukemia (affected in 3% of the tumors in panel)
- Identification of a gene, *Epi3*, which appears to cooperate with the loss of *Nf1* to cause acute myeloid leukemia (affected in 3% of the tumors in panel)
- Generation of a novel strain of mouse containing a deletion mutation of the alternatively spliced *Nf1*-exon 23a.

Reportable Outcomes

- Two abstracts presented at the National Neurofibromatosis Foundation meetings.
- Publication of two manuscripts (see Appendix).
- A repository of murine acute myeloid leukemia tumors
- Generation of a strain of mouse lacking the alternatively spliced *Nf1* exon 23a.
- Submission of a grant application to the NIH based on the identification of three genes which appear to cooperate with mutations in the *Nf1* gene to cause acute myeloid leukemia
- Granting of a Ph.D degree to my graduate student, Susan Blaydes, and successful placement in a postdoctoral position at the Florida Memorial Hospital
- Granting of a M.S. degree to my graduate student, Melissa Shelly, in addition to an M.B.A. degree, and successful placement in the insurance industry
- Successful placement of a former postdoctoral fellow, Tao Yang, in a pathology residency program in Brigham and Women's Hopital in Boston, MA

List of Personnel receiving pay from research effort

Camilynn Brannan
Susan Blaydes
Melissa Shelley
Joanne Anderson

Conclusions

Our hypothesis has been that progression of juvenile myelomonocytic leukemia (JMML) to acute leukemia (Gadner and Haas, 1992) is the result of genetic mutations in cooperating genes in addition to loss of *NF1*. During this study, we have successfully identified three loci that appear to be candidates for JMML to AML tumor progression. Therefore, this data strongly supports our hypothesis and has provided us with valuable reagents which we can use to experimentally prove our hypothesis.

So what does this research mean to NF1 patients? While most of the tumors associated with neurofibromatosis type 1 (NF1) are benign in nature, unfortunately, malignant transformation of a subset of NF1 tumors can be a serious complication. For example, plexiform neurofibromas are known to transform into malignant nerve sheath tumors (MNPSTs) and JMML is known to progress into acute leukemia (Gadner and Haas, 1992). Because of our research, we now have a handle on the types of genetic changes which lead to the formation, transformation and leukemic progression of NF1-associated JMML. This in turn may lead better prevention, diagnosis, and rational treatment for all malignancies that affect NF1 patients.

References

Andersen, L. B., Ballester, R., Marchuk, D. A., Chang, E., Gutmann, D. H., Saulino, A. M., Camonts, J., Wigler, M., and Collins, F. S. (1993). A conserved alternative splice in the von Recklinghausen neurofibromatosis (NF1) gene produces two neurofibromin isoforms, both of which have GTPase-activating protein activity., Mol Cell Biol *13*, 478-495.

Gadner, H., and Haas, O. A. (1992). Experience in pediatric myelodysplastic syndromes, Vol 6 (Philadelphia, W.B. Saunders Company).

Gutmann, D., Tennekoon, G. L., Cole, J., Collins, F. S., and Rutkowski, J. L. (1993). Modulation of neurofibromatosis type 1 gene product, neurofibromin, during Schwann cell differentation, J Neurosci Res *36*, 216-223.

Nishi, T., Lee, P. S., Oka, K., Levin, V. A., Tanase, S., Morino, Y., and Saya, H. (1991). Differential expression of two types of the neurofibromatosis type 1 (NF1) gene transcripts related to neuronal differentiation, Oncogene *6*, 1555-9.

Oh, I.-H. (1999). The *myb* gene family in cell growth, differentiation and apoptosis, Oncogene *18*, 3017-3033.

Wolff, L. (1996). Myb-induced transformation, Crit Rev Oncog *7*, 245-260.

Appendices

Costa, R.M., Yang, T. Huynh, D.P., Pulst, S.M., Viskochil, D.H., Silva, A.J. and Brannan, C.I. Learning deficits but normal development and tumor predisposition in mice lacking exon 23a of the Neurofibromatosis type 1 gene *Nature Genetics*, **27**, 399-405 (2001).

Blaydes, S.M., Kogan, S.C., Truong, B.-T. H., Gilbert, D.J., Copeland, N.G., Jenkins, N.A., Largaespada D.A., and Brannan, C.I. Retroviral integration at the *Epi1* locus cooperates with *Nf1* gene loss in the progression to acute myeloid leukemia *Journal of Virology,* **75**, 9427-9434 (2001).

Learning deficits, but normal development and tumor predisposition, in mice lacking exon 23a of *Nf1*

Rui M. Costa[1]*, Tao Yang[2,5]*, Duong P. Huynh[3], Stefan M. Pulst[3], David H. Viskochil[4], Alcino J. Silva[1] & Camilynn I. Brannan[2]

*These authors contributed equally to this work.

Neurofibromatosis type 1 (NF1) is a commonly inherited autosomal dominant disorder. Previous studies indicated that mice homozygous for a null mutation in *Nf1* exhibit mid-gestation lethality, whereas heterozygous mice have an increased predisposition to tumors and learning impairments. Here we show that mice lacking the alternatively spliced exon 23a, which modifies the GTPase-activating protein (GAP) domain of Nf1, are viable and physically normal, and do not have an increased tumor predisposition, but show specific learning impairments. Our findings have implications for the development of a treatment for the learning disabilities associated with NF1 and indicate that the GAP domain of NF1 modulates learning and memory.

Introduction

NF1 is a commonly inherited, autosomal dominant disorder that affects approximately 1 in 4,000 individuals. Mutations in the gene *NF1* cause several abnormalities in cell growth and tissue differentiation, including neurofibromas, café au lait spots and Lisch nodules of the iris[1,2]. A broad range of learning disabilities are also associated with NF1 (ref. 3). The protein encoded by *NF1*, neurofibromin, contains a GAP domain, known to inhibit Ras-mediated signal transduction[4–6]. Previous studies showed that mice homozygous for a *Nf1* null mutation exhibit mid-gestational lethality, whereas heterozygous mice have an increased tumor predisposition and learning impairments[7–9]. It is therefore unclear whether the learning disabilities are associated with developmental abnormalities or increased tumor predisposition. An alternatively spliced *NF1* exon, 23a, encodes 63 bp within the GAP-related domain. Exclusion of exon 23a results in the type I isoform, whereas inclusion of 23a results in the type II isoform. The type II isoform has a greater affinity for Ras, but lower GAP activity than type I (refs. 10,11). To determine the role of the type II isoform, we developed a mouse strain specifically lacking exon 23a ($Nf1^{tm1Cbr}$, hereafter $Nf1^{23a-/-}$). We found that mice homozygous for this mutation ($Nf1^{23a-/-}$) are viable and physically normal, and do not have an increased tumor predisposition. $Nf1^{23a-/-}$ mice, however, have specific learning impairments in hippocampal-dependent tasks (water maze and contextual discrimination) similar to those previously described for heterozygous null mutants[9]. These results demonstrate that the *Nf1* type II isoform is not required for either normal embryological development or tumor suppression, but is essential for normal brain function. Also, they indicate that the GAP-related domain of neurofibromin modulates learning and memory.

Results

Mice lacking exon 23a are viable and lack Nf1 type II

We made the exon 23a deletion vector by joining a DNA fragment located upstream of *Nf1* exon 23a to a fragment 3′ of exon 23a, generating a deletion of approximately 300 bp that included exon 23a (Fig. 1*a*). For positive selection of the targeting vector, a neomycin resistance cassette previously shown not to affect the transcription or splicing of the surrounding exons[12] was inserted in the deletion. After electroporation of the targeting vector and subsequent selection and screening of embryonic stem (ES) cell clones, 19 independent clones were identified that had the expected deletion of exon 23a.

Male chimeric mice were generated from two independent exon 23a deletion ES cell lines using standard procedures[13]. Upon maturity, males derived from each cell line were mated with C57BL/6J females, and germline transmission of the exon 23a deletion mutation was obtained from both lines. The resulting F_1 progeny were intercrossed to obtain F_2 mice of all three genotypes in the expected mendelian ratio. These (C57BL/6J×129/SvEv) F_2 animals were used in the experiments described below. Identical results were obtained from both independent lines; therefore, we combined them.

To confirm that the engineered mutation resulted in deletion of exon 23a, we used RT–PCR from RNA derived from brain tissue. We determined that the type II isoform was missing from $Nf1^{23a-/-}$ animals, but present in $Nf1^{23a+/+}$ and $Nf1^{23a+/-}$ animals (Fig. 1*b*). Moreover, $Nf1^{23a-/-}$ animals seemed to have normal levels of the type I isoform, indicating that the intronic neomycin resistance gene had no adverse affect on *Nf1* expression. Protein extracts prepared from brain tissue were analyzed by western-blot analysis using two affinity-purified

[1]*Departments of Neurobiology, Psychiatry and Psychology, BRI, UCLA, Los Angeles, California, USA.* [2]*Department of Molecular Genetics and Microbiology, Center for Mammalian Genetics, and the University of Florida Brain Institute, University of Florida College of Medicine, Gainesville, Florida, USA.* [3]*Cedars-Sinai Medical Center, UCLA School of Medicine, Los Angeles, California, USA.* [4]*Division of Medical Genetics, University of Utah, Salt Lake City, Utah, USA.* [5]*Present address: Brigham and Woman's Hospital, Boston, Massachusetts, USA. Correspondence should be addressed to A.J.S. (e-mail: Silvaa@mednet.ucla.edu) or C.I.B. (e-mail: Brannan@mgm.ufl.edu).*

anti-neurofibromin peptide antibodies[14]: NF1C, which recognizes the C terminus of neurofibromin; and GAP4, which recognizes the 21 amino acids encoded by exon 23a. We determined that, although all three genotypes express type I neurofibromin, only $Nf1^{23a+/+}$ and $Nf1^{23a+/-}$ mice express type II (Fig. 1*c*). These data demonstrate that the targeted deletion of *Nf1* exon 23a results in loss of type II neurofibromin. We then performed immunohistochemical analysis of brain tissue with the GAP4 antibody using $Nf1^{23a-/-}$ tissue as a negative control for antibody specificity. In contrast to previous studies using RT–PCR analysis of mouse cortical cultures[15], we found that type II neurofibromin is not only expressed in glia, but also in mature neurons in the mouse adult brain, including pyramidal neurons in the CA3 region of the hippocampus, Purkinje and granule cells in the cerebellum (Fig. 1*d–i*).

$Nf1^{23a-/-}$ mice do not have increased predisposition for tumor formation

We analyzed 28 adult mice (between the ages of 4 and 13 months; average 8 months) at the histopathological level (13 $Nf1^{23a-/-}$, 10 $Nf1^{23a+/-}$ and 5 $Nf1^{23a+/+}$). Complete examination revealed that only 4 of 28 mice had any abnormalities, but no abnormality was found more than once. One male $Nf1^{23a-/-}$ mouse (8 months) had an enlarged spleen (6 times normal) containing splenic hyperplasia with expansion of red pulp and increased extramedullar hematopoiesis. The lung, liver and kidneys revealed mild interstitial lymphocyte infiltrates. Another $Nf1^{23a-/-}$ male (13 months) had a small liver adenoma (0.3 cm) and a small lung adenoma (0.3 cm). A $Nf1^{23a-/-}$ female mouse (9 months) contained a large intra-abdominal cyst filled with yellow serous fluid. Microscopic examination revealed features consistent with endometriosis. Finally, a $Nf1^{23a+/-}$ male (6.5 months) had an enlarged kidney (2 times normal), which on sectioning revealed multiple cystic lesions in the medulla and seemed to be a renal cystadenoma. The remaining 24 mice were found to be completely normal, indicating that there are neither obvious genotype-associated pathologies nor an increased risk for malignancy within the first year of life.

Examination of brain sections from all 28 mice stained with hematoxylin and eosin revealed no gross or microscopic abnormalities among the three genotypes. As there have been reports of astrogliosis in individuals with NF1 and in $Nf1^{+/-}$ mice[16,17], we investigated the distribution of astrocytes in the brain by immunostaining with glial fibrillary acid protein (GFAP) antibody. Overall, no differences in the GFAP staining pattern or intensity were seen among the three groups of mice (data not shown).

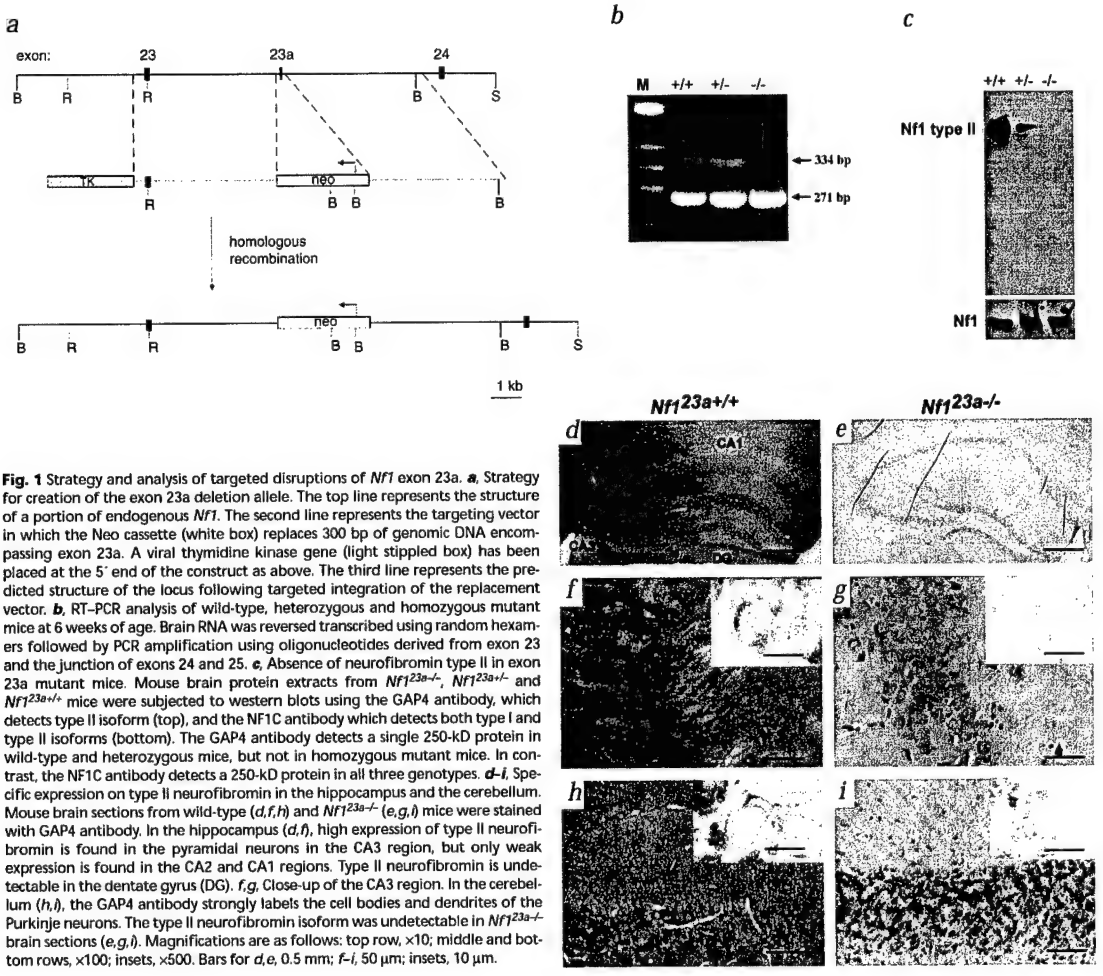

Fig. 1 Strategy and analysis of targeted disruptions of *Nf1* exon 23a. ***a***, Strategy for creation of the exon 23a deletion allele. The top line represents the structure of a portion of endogenous *Nf1*. The second line represents the targeting vector in which the Neo cassette (white box) replaces 300 bp of genomic DNA encompassing exon 23a. A viral thymidine kinase gene (light stippled box) has been placed at the 5′ end of the construct as above. The third line represents the predicted structure of the locus following targeted integration of the replacement vector. ***b***, RT–PCR analysis of wild-type, heterozygous and homozygous mutant mice at 6 weeks of age. Brain RNA was reversed transcribed using random hexamers followed by PCR amplification using oligonucleotides derived from exon 23 and the junction of exons 24 and 25. ***c***, Absence of neurofibromin type II in exon 23a mutant mice. Mouse brain protein extracts from $Nf1^{23a-/-}$, $Nf1^{23a+/-}$ and $Nf1^{23a+/+}$ mice were subjected to western blots using the GAP4 antibody, which detects type II isoform (top), and the NF1C antibody which detects both type I and type II isoforms (bottom). The GAP4 antibody detects a single 250-kD protein in wild-type and heterozygous mice, but not in homozygous mutant mice. In contrast, the NF1C antibody detects a 250-kD protein in all three genotypes. ***d–i***, Specific expression on type II neurofibromin in the hippocampus and the cerebellum. Mouse brain sections from wild-type (*d,f,h*) and $Nf1^{23a-/-}$ (*e,g,i*) mice were stained with GAP4 antibody. In the hippocampus (*d,f*), high expression of type II neurofibromin is found in the pyramidal neurons in the CA3 region, but only weak expression is found in the CA2 and CA1 regions. Type II neurofibromin is undetectable in the dentate gyrus (DG). *f,g*, Close-up of the CA3 region. In the cerebellum (*h,i*), the GAP4 antibody strongly labels the cell bodies and dendrites of the Purkinje neurons. The type II neurofibromin isoform was undetectable in $Nf1^{23a-/-}$ brain sections (*e,g,i*). Magnifications are as follows: top row, ×10; middle and bottom rows, ×100; insets, ×500. Bars for *d,e*, 0.5 mm; *f–i*, 50 μm; insets, 10 μm.

Because the *Nf1*$^{+/-}$ mice have increased predisposition for tumor formation and lower survival rates than wild-type controls[8], we aged another cohort of 27 mice (9 wild type, 10 *Nf1*$^{23a+/-}$, 8 *Nf1*$^{23a-/-}$) for over two years and analyzed their survival rates at different ages. No differences were observed in the survival rates of the different genotypes (Table 1; χ^2_6=2.27, P>0.05). At the age of 27 months, the surviving mice were euthanized and necropsy was performed. One wild-type female had pus in the abdominal cavity with enlarged spleen and one *Nf1*$^{23a-/-}$ male had a large (0.5 cm), well-confined mass in the prostate area, but no consistent pathology was seen among the three genotypes.

Table 1 • Survival rates of the different genotypes

Age (months)	12	18	24	27
Genotype				
wild type	100%	77%	77%	44%
Nf1$^{23a+/-}$	100%	100%	90%	50%
Nf1$^{23a-/-}$	100%	87.5%	75%	50%

We aged 27 mice (9 wild type, 10 *Nf1*$^{23a+/-}$ and 8 *Nf1*$^{23a-/-}$) to 27 months and analyzed their survival rates at different ages. No differences were observed in the survival rates of the different genotypes (χ^2_6=2.27, P>0.05).

Spatial learning is impaired in *Nf1*$^{23a-/-}$ mice

Visual-spatial problems are among the most common cognitive deficits detected in NF1 patients[3] and previous results showed that *Nf1*$^{+/-}$ mice have abnormal spatial learning[9]. To determine whether the *Nf1*$^{23a-/-}$ mutation affected spatial learning, we tested these mice in the hidden version of the water maze, a task known to be sensitive to hippocampal lesions[18]. In this task an animal learns to locate a submerged platform in a pool filled with opaque water. During training, mice were given 2 trials per day for 14 days. No differences were observed between wild-type and mutant mice in floating, thigmotaxic behavior or swimming speed (wild type=19.9 cm/s, mutants=18.9, $F_{1,22}$=0.297, P>0.05). Across days, all animals decreased the time taken to find the platform ($F_{1,21}$=13.914, P<0.05) and no difference was found between *Nf1*$^{23a-/-}$ mice and wild-type littermates ($F_{1,21}$=2.548, P>0.05; Fig. 2*a*). The time taken to find the platform during training is known to be a poor measure of spatial learning[19]. Therefore, we assessed spatial learning in probe trials in which the platform was removed from the pool. In a probe trial given after 10 days of training, the wild-type mice searched selectively, spending significantly more time searching for the platform in the quadrant where the platform was during training than in the other quadrants ($F_{3,44}$=12.242, P<0.05), whereas *Nf1*$^{23a-/-}$ mice searched randomly ($F_{3,44}$=2.716, P>0.05) and spent significantly less time searching for the platform in the training quadrant than wild type ($F_{3,22}$=6.555, P<0.05; Fig. 2*c*). Using another very sensitive measure to assess spatial learning[20] (proximity to platform), we verified that wild-type mice searched on average closer to the exact platform position than to the symmetrically opposite position in the pool (t_{11}=–2.612, P<0.05), whereas mutants did not (t_{11}=0.709, P>0.05; Fig. 2*e*).

Previous studies showed that additional training alleviates the learning deficits in the *Nf1*$^{+/-}$ mice[9]. Consistently, following four additional days of training, the *Nf1*$^{23a-/-}$ mice searched as selectively as wild-type controls in a probe test (F=1.301, P>0.05; Fig. 3*d*). They spent significantly more time searching in the training quadrant than in the other quadrants ($F_{3,44}$=15.348, P<0.05) and searched closer to the exact platform position (t_{11}=–2.905, P<0.05; Fig. 3*f*).

To determine whether deficits in motivation, motor coordination, or vision account for the abnormalities in spatial learning,

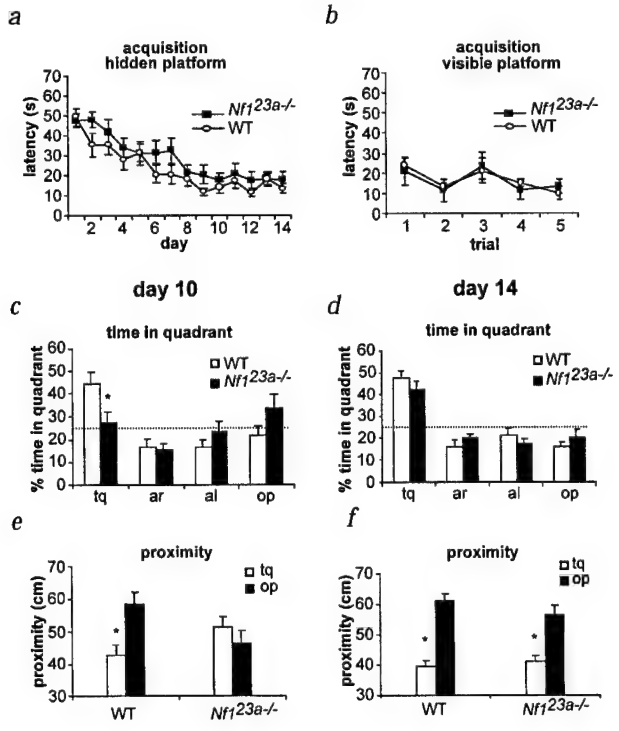

Fig. 2 Spatial learning in the water maze. ***a***, *Nf1*$^{23a-/-}$ mice (n=12) and wild-type littermates (n=12) were trained for 14 d, with 2 trials per day in the water maze. The average latency to reach the hidden platform is plotted. Escape latencies decrease across days ($F_{1,21}$=13.914, P<0.05) and there is no difference in latencies between mutants and controls during training ($F_{1,21}$=2.548, P>0.05). ***b***, After the hidden version of the water maze, the animals were run in the visible platform task. There was no difference in latency to get to the platform across trials between wild-type and mutants ($F_{1,14}$=0.30, P>0.05). ***c***, Results of a probe trial given after 10 days of training. The percentage of time animals spent searching in each of the training quadrants is shown. ANOVA shows that there is an effect of percentage time spent in quadrant for wild type ($F_{3,44}$=12.242, P<0.05). Post-hoc analysis show that wild-type mice spent significantly more time searching in the training quadrant than in any of the other quadrants (Fisher PLSD, P<0.05). Mutants did not search selectively in any of the quadrants ($F_{3,44}$=2.716, P>0.05) and spent significantly less time searching in the training quadrant than wild type ($F_{1,22}$=6.555, P<0.05). ***d***, Probe trial given after 14 days of training. Both mutants ($F_{3,44}$=15.348, P<0.05) and wild type ($F_{3,44}$=23.110, p<0.05) searched selectively and spent significantly more time searching in the training quadrant than in any of the other quadrants (Fisher PLSD, P<0.05). ***e***, During the probe trial given at day 10, wild-type mice searched on average closer to the exact position of the platform during training than to the symmetric position in the opposite quadrant (t_{11}=–2.612, P<0.05), whereas mutants did not (t_{11}=0.709, P>0.05). ***f***, Probe trial day 14. Both mutants and wild type searched on average closer to the exact platform position than to the opposite position in the pool (t_{11}=–2.905, P<0.05; t_{11}=–6.71, P<0.05). Dashed line indicates random search (25% in each quadrant). *Significant difference, P<0.05. tq, training quadrant; ar, adjacent right quadrant; al, adjacent left quadrant; op, opposite quadrant.

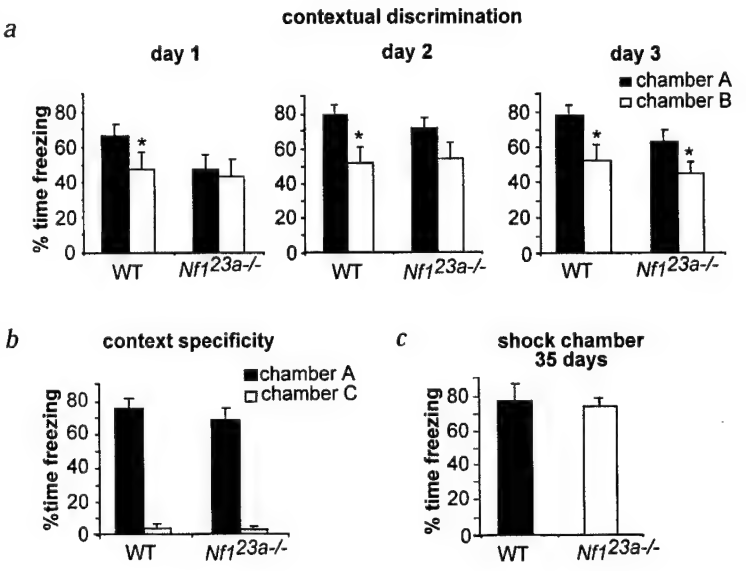

Fig. 3 Contextual discrimination. ***a***, Percentage of time spent freezing in chamber A (shock context, filled) versus chamber B (no-shock context, open bars) shown for each of the three testing days. Wild-type mice spent significantly more time freezing in the chamber where they were shocked than in the other chamber on each test day (day 1, A=66.8, B=47.4, t_8=2.407, P<0.05; day 2 A=78.0, B=51.2, t_8=5.873, P<0.05; day 3, A=77.2, B=52.2, t_8=4.890, P<0.05), showing that they discriminate between the two chambers. *Nf1*$^{23a-/-}$ mutants did not discriminate between the chambers (day 1, A=47.5, B=43.3, t_8=0.603, P>0.05; day 2, A=70.5 B=53.5, t_8=1.839, P>0.05) during the first two days of training, but they finally discriminated after three days of training (A=62.4, B=44.8, t_8=2.534, P<0.05). ***b***, Specificity of the conditioned freezing. After training in contexts A and B, mutants and wild-type mice were tested in chamber A and a novel chamber, C. Both mutants (A=66.6, C=3.1) and wild-type (A=73.7,C=3.8) showed similarly robust freezing in chamber A (shock context, black bars, $F_{1,15}$=0.637, P>0.05) and essentially no freezing in chamber C (novel context, gray bars, $F_{1,15}$=0.111, P>0.05). ***c***, Memory consolidation does not seem to be impaired in the mutants because both mutant (open bars) and wild-type controls (filled bars) exhibited similar levels of freezing (wild type=77.1, mutants=73.5, $F_{1,15}$=0.111, P>0.05) when re-exposed 35 days later to the same chamber where they were shocked. *Significant difference, P<0.05.

the same animals were tested in the visible platform version of the water maze, a task that is not affected by hippocampal lesions[18]. In this task, animals must locate a platform marked with a visible cue. Both mutant and wild-type control mice acquired the task similarly, as the times taken to reach the visible platform were not different between the groups ($F_{1,14}$=0.030, P>0.05, Fig. 3*b*).

Nf1$^{23a-/-}$ mice are impaired in contextual discrimination

We confirmed the water maze results using another hippocampal-dependent task, contextual discrimination[21]. In this task animals are required to discriminate between two similar chambers, one in which they receive a mild foot shock (chamber A) and another in which they do not (chamber B). Contextual discrimination is assessed by measuring the time spent 'freezing' (that is, without any bodily movement aside from respiration) in each chamber. Throughout training, wild-type mice froze significantly more in the chamber where they were shocked than in the other chamber (P<0.05 for all three days), showing that they discriminate between the two chambers (Fig. 3*a*). In contrast, during the first two days of training, *Nf1*$^{23a-/-}$ mutants did not discriminate between the chambers (P>0.05 for both days). *Nf1*$^{23a-/-}$ mice finally discriminated between the chambers after three days of training (day 3, t_8=–2.534, P<0.05), confirming that, just as with spatial learning, additional training can overcome the learning deficits. When tested in chamber C, which is very different from the training chambers, both wild-type and mutant mice showed little or no freezing (Fig. 3*b*). This demonstrates that the freezing responses in chamber B are probably triggered by the cues shared with chamber A. The *Nf1*$^{23a-/-}$ mutation does not seem to affect long-term memory, because mutants and controls had similar levels of freezing ($F_{1,15}$=0.111, P>0.05) when tested 35 days after training (Fig. 3*c*). Also, the ability to freeze seems to be unaffected by the mutation. In chamber A, both baseline freezing (wild type, 9.0; *Nf1*$^{23a-/-}$, 6.7; $F_{1,15}$=0.264, P>0.05) and freezing after foot-shock delivery ($F_{1,15}$=3.495, P>0.05) were similar between wild type and mutants.

Nf1$^{23a-/-}$ mice have delayed acquisition of motor skills

Some individuals with NF1 show delayed acquisition of motor skills and motor coordination problems[3]. To determine whether the *Nf1*$^{23a-/-}$ mutation affects motor function, we tested the mice on an accelerating rota-rod[22,23] (4–40 r.p.m. in 300 s). *Nf1*$^{23a-/-}$ mice fell off the rotating rod sooner than wild-type mice ($F_{1,17}$=4.84, P<0.05; Fig. 4*a*). This motor coordination impairment is not due to greater fatigue in the mutants because, at an intermediate, constant speed (14 r.p.m), mutants and controls showed no differences in latency to fall from the rotating rod ($F_{1,16}$=0.262, P>0.05; Fig. 4*b*).

The effects of the *Nf1*$^{23a-/-}$ mutation are specific

It is unlikely that the learning deficits in these mice are caused by generalized neurological problems or poor motor performance, as swimming speed, ability to freeze, ambulance (hind paw analysis[23]), exploratory behavior (open field[23]), muscular strength (wire hang[24]) and body weight (data not shown) were not affected by the mutation.

Just as NF1 patients do not show learning deficits in all tasks, the *Nf1*$^{23a-/-}$ mutation did not affect all forms of learning. When tested in the social transmission of food preferences[25], a task that assesses the capability of an animal to remember a food smelled in the breath of a littermate, *Nf1*$^{23a-/-}$ mice learned as well as wild-type controls (t_8=3.23, P<0.05; Fig. 5). This is relevant because the brain regions required to solve this task[26] are different from the ones required for the water maze[18] and contextual discrimination[21], revealing that the effects of this mutation are specific.

Discussion

Neurofibromin is a complex protein that is implicated in a number of biological processes, including growth, differentiation, learning and memory. Accordingly, inactivating mutations of *NF1* in humans and mice results in a wide spectrum of symptoms ranging from increased tumor predisposition to learning disabilities[27]. *NF1* encodes several distinct isoforms of neurofibromin.

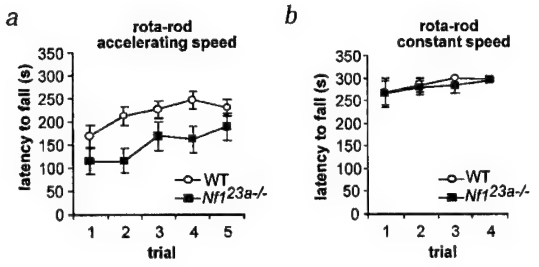

Fig. 4 Motor performance in the rota-rod. ***a***, Accelerating rota-rod. Wild-type and *Nf1*$^{23a-/-}$ were given 5 trials in an accelerating rota-rod (4–40 r.p.m. in 5 min) during 1 day. All subjects showed an increase in the latency to fall across trials ($F_{1,17}$=13.3, P<0.05) indicating that they improved their performance across trials. In average mutants fell off the rotating rod sooner than the wild type ($F_{1,17}$=4.84, P<0.05). ***b***, Constant speed rota-rod. The mice were given four trials at a lower constant speed (14 r.p.m. for 5 min) during one day. Under these conditions, mutants and controls showed no differences in latency to fall from the rotating rod ($F_{1,16}$=0.262, P>0.05).

Here we have demonstrated that one isoform, type II, is important for brain function, but not for embryological development or tumor suppression. It is possible that other alternatively spliced exons (such as exon 9a) expressed postnatally in forebrain neurons[28], also have a role in mechanisms underlying learning and memory. Our data indicate that the learning deficits caused by mutations that inactivate *NF1* in mice and humans are not a result of developmental deficits or undetected tumors. Instead, they suggest that the learning deficits in individuals with NF1 are caused by the disruption of neurofibromin function in the adult brain, a finding with important implications for the development of a treatment for the learning disabilities associated with NF1.

Exon 23a modifies the GAP domain of NF1. Thus, our results indicate that modulation of the Ras pathway is important to learning and memory. These data are consistent with previous findings. First, patients carrying a missense mutation that specifically eliminates the Ras-GAP activity of neurofibromin have learning disabilities[29]. Second, pharmacological disruption of the downstream Ras target MAPK disrupts learning in rodents[30]. Third, a deletion mutation of Ras guanine-nucleotide-exchange factor (Ras-GRF) also affects learning and memory in mice[31]. In addition, *Nf1*-null mutations are known to elevate Ras-GTP (refs. 32,33), and cause learning disabilities[9]. These results suggest that either abnormally high or low Ras-GTP levels affect learning and memory. It has been shown that type I neurofibromin has higher GAP activity and lower affinity for Ras than type II (refs. 10,11), offering the possibility that the ratio between the two isoforms modulates Ras signaling. Because *Nf1* type I and type II isoforms are expressed in some of the same populations of cells in the adult brain, and the relative expression of these two isoforms in neuronal cultures is subject to modulation by extrinsic factors, such as NGF (ref. 34), we propose that differential expression of these two isoforms may have a role in fine-tuning Ras activity in the central nervous system.

Although the neurological and cognitive deficits associated with NF1 are pleiomorphic and incompletely penetrant (only about half of individuals show learning disabilities), spatial problems are the most common abnormality associated with this condition. Although it is unclear whether the same brain systems underlie the spatial phenotype in mice and humans, it is important to note that both the heterozygous null *Nf1* mutation and the *Nf1*$^{23a-/-}$ mutation primarily result in incompletely penetrant spatial learning deficits in mice. Additionally, *NF1* mutations can result in motor coordination problems in both mice and humans. These compelling parallels demonstrate the usefulness of mouse models to understand the etiology of learning deficits in NF1.

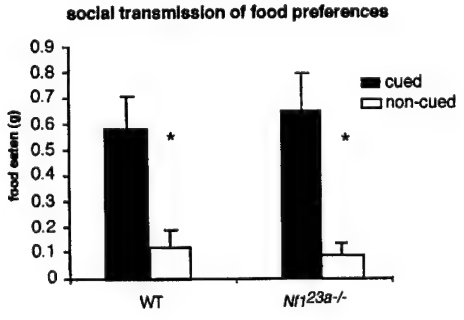

Fig. 5 Social transmission of food preferences. After 15 min of interaction with demonstrator mice, both wild-type and mutant mice showed robust socially transmitted food preference (wild type, cued=0.58 g, non-cued=0.12 g, t_8=3.16, P<0.05; *Nf1*$^{23a-/-}$, cued=0.65 g, non-cued=0.09 g, t_8=3.23, P<0.05). Even with shorter interaction times (5 min), no differences were observed between mutant and wild-type mice (data not shown).

Methods

Targeted deletion of exon 23a. The exon 23a deletion vector was made by joining a 5′ upstream 4.8 kb *Bsr*FI fragment containing exon 23 to a 3′ downstream 4.6 kb *Bst*BI-(*Not*I) fragment containing intronic sequence. This resulted in a deletion of approximately 300 bp of genomic DNA, which included exon 23a. A neomycin selectable marker (KT3NP4) was inserted between the two fragments in the opposite transcriptional orientation relative to *Nf1* and a PGK-TK cassette was placed at the 5′ end of the construct. CJ.7 cells[35] were cultured and electroporated with linearized vector using standard conditions[36], and then plated onto gelatin coated dishes in media containing ESGRO (1,000 μ/ml; Gibco BRL). After 24 h, the culture medium was changed to include 250 μg/ml active concentration of Geneticin (Gibco BRL). After 48 h it was changed again to include 0.7 μM FIAU (0.7 μM; Oclassen Pharmaceuticals). Seven days after electroporation, 500 Geneticin- and FIAU-resistant colonies were picked and expanded on mouse embryo fibroblasts in the presence of Geneticin. We isolated genomic DNA from ES cells as described[37]. Aliquots of the DNA (5 μg) were digested to completion with *Bam*HI, then electrophoresed through 0.8% agarose gels, transferred to Hybond nylon membranes (Amersham) and subsequently screened using a 0.5-kb *Eco*RI-*Spe*I fragment mapping 5′ to the limit of homology. Autoradiography was carried out at –70 °C using Kodak XAR film. We found the expected replacement event in 1 of every 9 clones. We selected two independent clones to derive chimeric mice according to standard procedures[13].

RT–PCR. We pretreated total brain RNA (10 μg) with DNase I (Gibco BRL). Half of the reaction was subsequently used to synthesize first-strand cDNA with Superscript II reverse transcriptase (Gibco BRL) and random primers (Gibco BRL). The other half of the reaction was manipulated in parallel in the absence of RT. We used one-twentieth of the +RT or –RT reactions to program PCR reactions using the following conditions: 10 mM Tris-HCl, pH 8.3, 50 mM KCl, 1.5 mM $MgCl_2$, 0.125 mM of the four dNTPs, 1 unit *Taq* DNA polymerase (Boehringer) and 4 μM each of the primers 5′–GCGGAACCTCCTTCAGATGACTG–3′ and 5′–GCTCTGAAGTACCTTTGAC–3′. PCR amplification conditions were as follows: 95 °C for 4 min, followed by 40 cycles of 94 °C for 1 min, 55 °C for 1 min, and 72 °C for 2 min. The final cycle was followed by a 10-min extension period at 72 °C.

Genotyping. To genotype genomic DNA isolated from the exon 23a deletion mice, we used three oligonucleotide primers: Nf23a,

5′–GCAACTTGCCACTCCCTACTGAATAAAGCTACAGTAAAA–3′; intron 23a, 5′–CCACTCACATGACCCGCAAACG–3′; and KT3NP4, 5′–GGAGTTGTTGACGCTAGGGCTC–3′. PCR conditions were the same as above except of the following changes: 25 µl reactions were used containing 400 ng each of the 3 oligonucleotide primer. PCR of DNA from wild-type animals resulted in a 450-bp fragment; from homozygous mutant animals, a 520-bp fragment; and from heterozygous animals, both a 450-bp and a 520-bp fragment.

Western blot. Mouse brains were homogenized in triple detergent buffer (100 mM Tris-HCl, pH 8.0, 150 mM NaCl, 1% Triton X-100, 0.5 mM deoxycholic acid, 1% SDS, 50 ng/ml Pefabloc, 2 U/ml aprotinin, 1 mM EGTA, 2 µg/ml pepstatin) and spun for 1 h at 100,000*g* at 4 °C. Protein concentration was determined using the Bradford Protein Detection kit (Biorad). Western blots were performed on the same day of protein extraction by first precipitating protein extracts (100 µg) with acetone, which was then dissolved in 1×SDS–PAGE sample buffer and run on a 4–20% premade SDS–PAGE (Biorad) for 1 h. Proteins were then transferred to Amersham nitrocellulose filter overnight at 4 °C in western-blot buffer. The filters were then probed with either GAP4 or NF1C antibodies (1 µg/ml) using a chemiluminescent kit according to manufacturer's instructions (Amersham). Both GAP4 and NF1C were previously characterized[14].

Pathology. Age- and sex-matched adult mice were killed and internal organs removed for analysis. After gross examination, the tissues were fixed in 10% neutral buffered formalin. Representative tissue sections were dehydrated, embedded in paraffin, sectioned (5 µm), mounted on slides and stained with hematoxylin and eosin.

Imunohistochemistry. For the GAP4 antibody imunohistochemistry, the mice were infused through the heart with DPBS, followed by 2% paraformaldehyde in DPBS. The brains were then removed and processed for paraffin embedding. We cut 5-µm sections. Sections were boiled in sodium citrate (10 mM, pH 6) for 10 min to unmask the GAP4 antigenic site, blocked with avidin/biotin and 3% normal goat serum. Sections were then incubated with affinity-purified GAP4 antibody[14] overnight at 4 °C. Primary antibodies were detected using the Vector rabbit ABC elite Peroxidase kit (Vector), enhanced by DAB enhancer, and visualized with diaminobenzidine (DAB) (Biomedia). The sections were then counterstained with aqueous hematoxylin (Xymed). The same basic procedure was used for GFAP staining using an automated immunohistochemistry stainer (Ventana Medical System 320, and rabbit anti-cow GFAP antibody (Dakopatts) at 1:1,200 dilution as a primary antibody.

Animals. For the behavioral experiments, we used group-housed males and females. The experimenters were blind to the genotype of each animal during the experiments. All the protocols used were approved by UCLA's Animal Research Committee.

Water maze. The basic protocol for the water maze experiments has been described[38]. Our pool is circular with a 1.2-m diameter and the platform has an 11-cm diameter. The water is made opaque with non-toxic white paint and maintained at 27 °C. The movement of the mice is processed by a digital tracking device (VP118, HVS Image). During the hidden platform test, the platform was submerged (1 cm) below the water surface and maintained in the same place throughout training. The mice were given 2 trials every day (60 s ITI) for 14 d and the starting position was varied from trial to trial. In the probe trials given after 10 and 14 d of training, the platform was removed and the mice were allowed to search for it for 60 s. In the visible platform test, a distinct symmetrical cue (black and white golf ball) was fixed 5 cm above the center of the submerged platform. The animals were given 5 trials during 1 day (30 min ITI); the starting position and the platform location were pseudo-randomly varied from trial to trial.

Contextual discrimination. The contextual discrimination experiments were performed as described[21]. Chambers A and B were similar, both with grid floors and located in sound attenuating boxes in dimly lit rooms located outside the vivarium; and they were modified to have some unique features (location, geometry, background noise, odor). Chamber C, which shared no obvious cues with chambers A and B, was located in a room inside the mouse vivarium and was brightly illuminated. This experiment consisted of three stages: pre-exposure (1 d), training (1 d) and testing (3 d). Each mouse was habituated to contexts A and B for 10 min before training started (day –1). The next day (day 0) animals were placed in chambers A and B for 3 min (the order was balanced), and after 150 s a mild foot-shock (0.75 mA for 2 s) was delivered in chamber A but not in chamber B. During the 3 consecutive testing days animals were placed in each chamber and the amount of freezing during the initial 150 s was measured. Freezing was assessed every 5 s: mice were scored as freezing if they were immobile (cessation of all bodily movement aside from respiration) for 2 s. On each of the testing days animals were shocked after 150 s in chamber A but not in chamber B. Context specificity was tested 24 h after the end of the contextual discrimination task by placing the animals in chambers A and C and measuring the amount of freezing. Long-term memory was assessed 35 d after the end of the contextual discrimination task.

Rota-rod. For the accelerating rota-rod task using a rota-rod (Ugo Basile 7650) accelerating from 4 to 40 r.p.m. in 300 s. 5 trials (35 min ITI) during the same day were given. For the constant speed rota-rod task, animals were given 4 trials (5 min) during the same day, with the rota-rod rotating at 14 r.p.m. The latency for the animals to fall from the rota-rod was measured. If the mice initiated passive rotation (that is, grabbed the rotating rod with all four paws and avoid falling) that was considered a fall.

Social transmission of food preferences. This task was performed as described[25,26]. Mice were shaped to eat ground chow from a metal cup. First, a demonstrator mouse was removed from each cage and food deprived for 24 h. The demonstrator mouse was then allowed to eat scented food for 1 h and placed back in the cage for a period of 15 min to interact with the other mice in the cage (observers). After this, observers were food-deprived for 24 h. Finally, observer mice were tested for their preference in a 1-h test in which they had a choice between the food they smelled on the demonstrator's breath and another scented food. The amount of each food eaten (g) was measured. The demonstrated scents were pseudo-randomly assigned to each cage of mice.

Statistical analysis. A two-way ANOVA with repeated measures was used to analyze the acquisition data from the water maze and rota-rod tasks. To analyze the performance in the water maze probe trials we used a single-factor ANOVA on the percentage time in quadrant; post-hoc comparisons between quadrants were performed when there was an effect of quadrant. Planned comparisons using a paired *t*-test were used to analyze the contextual discrimination data, the proximity data in the water maze and the social transmission of food preference data.

Acknowledgments

We thank K. Thomas for the KT3NP4 neomycin cassette; R. White for support in the generation of the GAP4 antibody; D.H. Gutmann for help interpreting the immunohistochemistry; P.W. Frankland for discussions; and C.M. Spivak for inspiration and support. R.C.M. is supported by the GABBA Graduate Program (Oporto University) and the Portuguese Foundation for Science and Technology (BD 13854/97). This work was supported by a grant from the Department of Defense, U.S. Army Medical Research and Materiel Command (DAMD17-97-1-7339) to C.I.B.; grants from the NIH (R01 NS38480), the Neurofibromatosis Consortium and the Neurofibromatosis Foundation to A.J.S.; and a donation from C.M. Spivak to A.J.S.

Received 11 December 2000; accepted 26 January 2001.

1. Gutmann, D.H. & Collins, F.S. von Recklinghausen neurofibromatosis. *The Metabolic and Molecular Basis of Inherited Disease* 1–19 (McGraw Hill, New York, 1994).
2. Huson, S.M. & Hughes, R.A.C. *The Neurofibromatoses: A Pathogenic and Clinical Overview* (Chapman & Hall, London, 1994).
3. Ozonoff, S. Cognitive impairment in neurofibromatosis type 1. *Am. J. Med. Genet.* **89**, 45–52 (1999).
4. Ballester, R. *et al.* The NF1 locus encodes a protein functionally related to mammalian GAP and yeast IRA proteins. *Cell* **63**, 851–859 (1990).
5. Martin, G.A. *et al.* The GAP-related domain of the neurofibromatosis type 1 gene product interacts with *ras* p21. *Cell* **63**, 843–849 (1990).

6. Xu, G.F. *et al.* The catalytic domain of the neurofibromatosis type 1 gene product stimulates ras GTPase and complements ira mutants of S. cerevisiae. *Cell* **63**, 835–841(1990).
7. Brannan, C.I. *et al.* Targeted disruption of the neurofibromatosis type-1 gene leads to developmental abnormalities in heart and various neural crest-derived tissues. *Genes Dev.* **8**, 1019–1029 (1994).
8. Jacks, T. *et al.* Tumour predisposition in mice heterozygous for a targeted mutation in *Nf1*. *Nature Genet.* **7**, 353–361 (1994).
9. Silva, A.J. *et al.* A mouse model for learning and memory deficits associated with neurofibromatosis type 1. *Nature Genet.* **15**, 281–284 (1997).
10. Andersen, L.B. *et al.* A conserved alternative splice in the von Recklinghausen neurofibromatosis (NF1) gene produces two neurofibromin isoforms, both of which have GTPase-activating protein activity. *Mol. Cell. Biol.* **13**, 478–495 (1993).
11. Viskochil, D.H. Gene structure and function. in *Neurofibromatosis Type 1: From Genotype to Phenotype* (eds. Upadhyaya, M. & Cooper, D.N.) 39–56 (Bios Scientific Publishers, Oxford, 1998).
12. Zeiher, B.G. *et al.* A mouse model for the delta F508 allele of cystic fibrosis. *J. Clin. Invest.* **96**, 2051–2064 (1995).
13. Hogan, B., Beddington, R., Constantini, F. & Lacy, E. *Manipulating the Mouse Embryo: A Laboratory Manual* (Cold Spring Harbor Laboratory Press, New York, 1994).
14. Huynh, D.P., Nechiporuk, T. & Pulst, S.M. Differential expression and tissue distribution of type I and type II neurofibromins during mouse fetal development. *Dev. Biol.* **161**, 538–551 (1994).
15. Gutmann, D.H., Cole, J.L. & Collins, F.S. Expression of the neurofibromatosis type 1 (NF1) gene during mouse embryonic development. *Prog. Brain Res.* **105**, 327–335 (1995).
16. Nordlund, M.L., Rizvi, T.A., Brannan, C.I. & Ratner, N. Neurofibromin expression and astrogliosis in neurofibromatosis (type I) brains. *J. Neuropath. Exp. Neurol.* **54**, 588–600 (1995).
17. Rizvi, T.A. *et al.* Region-specific astrogliosis in brains of mice heterozygous for mutations in the neurofibromatosis type I (Nf1) tumor suppressor. *Brain Res.* **816**, 111–123 (1999).
18. Cho, Y. & Silva, A.J. Ibotenate lesions of the hippocampus impair spatial learning but not contextual fear conditioning in mice. *Behav. Brain Res.* **98**, 77–87 (1999).
19. Brandeis, R., Brandys, Y. & Yehuda, S. The use of the Morris water maze in the study of memory and learning. *Int. J. Neurosci.* **48**, 29–69 (1989).
20. Gallagher, M., Burwell, R. & Burchinal, M. Severity of spatial impairments in aging: development of a spatial index for performance in the Morris water maze. *Behav. Neurosci.* **107**, 618–626 (1993).
21. Frankland, P.W., Cestari, V., Filipkowski, R.K., McDonald, R.J. & Silva, A.J. The dorsal hippocampus is essential for context discrimination but not for contextual conditioning. *Behav. Neurosci.* **112**, 863–874 (1998).
22. Chen, C. *et al.* Impaired motor coordination correlates with persistent multiple climbing fiber innervation in PKCg mutant mice. *Cell* **83**, 1233–1242 (1995).
23. Barlow, C. *et al.* *Atm*-deficient mice: a paradigm of ataxia telangietasia. *Cell* **86**, 159–171 (1996).
24. Lijam, N. *et al.* Social interaction and sensimotor gating abnormalities in mice lacking *Dvl1*. *Cell* **90**, 895–905 (1997).
25. Kogan, J.H. *et al.* Spaced training induces normal long-term memory in CREB mutant mice. *Curr. Biol.* **7**, 1–11 (1997).
26. Bunsey, M. & Eichenbaum, H. Selective damage to the hippocampal region blocks long-term retention of a natural and non-spatial stimulus-stimulus association. *Hippocampus* **5**, 546–556 (1995).
27. Upadhyaya, M. & Cooper, D.N. (eds.) *Neurofibromatosis Type 1: From Genotype to Phenotype* (Bios Scientific Publisher, Oxford, 1998).
28. Gutmann, D.H., Zhang, Y. & Hirbe, A. Developmental regulation of a neuron-specific neurofibromatosis type 1 isoform. *Ann. Neurol.* **46**, 777–782 (1999).
29. Klose, A. *et al.* Selective disactivation of neurofibromin GAP activity in neurofibromatosis type 1. *Hum. Mol. Genet.* **7**, 1261–1268 (1998).
30. Atkins, C.M., Selcher, J.C., Petraitis, J.J., Trzaskos, J.M. & Sweatt, J.D. The MAPK cascade is required for mammalian associative learning. *Nature Neurosci.* **1**, 602–609 (1998).
31. Brambrilla, R. *et al.* A role for the Ras signalling pathway in synaptic transmission and long term memory. *Nature* **390**, 281–286 (1997).
32. Largaespada, D.L., Brannan, C.I., Jenkins, N.A. & Copeland, N.G. *Nf1* deficiency causes Ras-mediated granulocyte/macrophage stimulating factor hypersensitivity and chronic myeloid leukemia. *Nature Genet.* **12**, 137–143 (1996).
33. Bollag, G. *et al.* Loss of *Nf1* results in activation of the Ras signalling pathway and leads to aberrant growth in hematopoietic cells. *Nature Genet.* **12**, 144–148 (1996).
34. Metheny, L.J. & Skuse, G.R. NF1 mRNA isoform expression in PC12 cells: modulation by extrinsic factors. *Exp. Cell Res.* **228**, 44–49 (1996).
35. Swiatek, P.J. & Gridley, T. Perinatal lethality and defects in hindbrain development in mice homozygous for a targeted mutation of the zinc finger gene Krox20. *Genes Dev.* **7**, 2071–2084 (1993).
36. Robertson, E.J. Embryo-derived stem cells. in *Teratocarcinomas and Embryonic Stem Cells: A Practical Approach* (ed. Robertson, E.J.) 71–112 (IRL, Oxford, 1987).
37. Laird, P.W. *et al.* Simplified mammalian DNA isolation procedure. *Nucleic Acids Res.* **19**, 4293–4294 (1991).
38. Bourtchuladze, R. *et al.* Deficient long-term memory in mice with a targeted mutation of the cAMP-responsive element-binding protein. *Cell* **79**, 59–68 (1994).

JOURNAL OF VIROLOGY, Oct. 2001, p. 9427–9434 Vol. 75, No. 19
0022-538X/01/$04.00+0 DOI: 10.1128/JVI.75.19.9427–9434.2001

Retroviral Integration at the *Epi1* Locus Cooperates with *Nf1* Gene Loss in the Progression to Acute Myeloid Leukemia

SUSAN M. BLAYDES,[1] SCOTT C. KOGAN,[2] BAO-TRAN H. TRUONG,[2] DEBRA J. GILBERT,[3] NANCY A. JENKINS,[3] NEAL G. COPELAND,[3] DAVID A. LARGAESPADA,[4] AND CAMILYNN I. BRANNAN[1]*

Department of Molecular Genetics and Microbiology, Center for Mammalian Genetics, and University of Florida Shands Cancer Center, University of Florida College of Medicine, Gainesville, Florida 32610[1]; Department of Laboratory Medicine, Comprehensive Cancer Center, University of California—San Francisco, San Francisco, California 94143[2]; Mouse Cancer Genetics Program, National Cancer Institute—Frederick, Frederick, Maryland 21702[3]; and Department of Genetics, Cell Biology and Development, University of Minnesota Cancer Center, Minneapolis, Minnesota 55455[4]

Received 29 March 2001/Accepted 19 June 2001

Juvenile myelomonocytic leukemia (JMML) is a disease that occurs in young children and is associated with a high mortality rate. In most patients, JMML has a progressive course leading to death by virtue of infection, bleeding, or progression to acute myeloid leukemia (AML). As it is known that children with neurofibromatosis type 1 syndrome have a markedly increased risk of developing JMML, we have previously developed a mouse model of JMML through reconstitution of lethally irradiated mice with hematopoietic stem cells homozygous for a loss-of-function mutation in the *Nf1* gene (D. L. Largaespada, C. I. Brannan, N. A. Jenkins, and N. G. Copeland, Nat. Genet. 12:137–143, 1996). In the course of these experiments, we found that all these genetically identical reconstituted mice developed a JMML-like disorder, but only a subset went on to develop more acute disease. This result strongly suggests that additional genetic lesions are responsible for disease progression to AML. Here, we describe the production of a unique tumor panel, created using the BXH-2 genetic background, for identification of these additional genetic lesions. Using this tumor panel, we have identified a locus, *Epi1*, which maps 30 to 40 kb downstream of the *Myb* gene and appears to be the most common site of somatic viral integration in BXH-2 mice. Our findings suggest that proviral integrations at *Epi1* cooperate with loss of *Nf1* to cause AML.

Juvenile myelomonocytic leukemia (JMML) is a disease characterized by a young age of onset, a tendency to affect boys, prominent enlargement of the liver and spleen, leukocytosis, and the absence of the Philadelphia chromosome. JMML has a poor prognosis, with either progression to acute myeloid leukemia (AML) or death from bleeding or infection (36). It has been estimated that at least 10% of children with JMML also have neurofibromatosis type 1 (NF1) syndrome, an autosomal dominant disorder found in 1/3500 individuals (1, 7, 14, 32). However, the actual frequency of children with NF1 and JMML is likely higher than 10% as the peak incidence of childhood leukemia occurs at an age when NF1 often goes undiagnosed (13, 34). In fact, one study found that 15% of JMML patients had mutations in the *NF1* gene even though there was no previous clinical diagnosis of NF1 (33), suggesting that approximately 25% of JMML cases are associated with NF1.

While *RAS* gene point mutations are commonly found in JMML patients without NF1, they are not found in JMML patients with NF1 (20), providing genetic evidence that *NF1* and *RAS* are involved in the same pathway. This idea is supported by the fact that neurofibromin, the protein product of *NF1*, contains a region that has extensive homology with the catalytic domain of GTPase activating proteins that are known to accelerate the intrinsic GTPase activity of Ras, thereby negatively regulating Ras GTP levels (15). This suggests that inactivating mutations in *NF1* are equivalent to activating mutations in *RAS*. Consistent with the hypothesis, analysis of bone marrow taken from children with NF1 and JMML revealed that close to half of the samples had somatic loss of heterozygosity (LOH) for markers within and near the *NF1* locus (31). In these LOH samples, it was determined that the somatic deletion removed the remaining normal *NF1* allele. Together, these results indicated that homozygous *NF1* loss predisposes myeloid cells to leukemic transformation in children by activation of the Ras pathway.

To examine the direct consequence of loss of *NF1* in the hematopoietic lineage, we previously developed a mouse model for NF1-associated JMML (22). This model relied on reconstitution of lethally irradiated mice with hematopoietic stem cells homozygous for a mutant *Nf1* allele, $Nf1^{Fcr}$, in which an insertion mutation in exon 31 results in the formation of a null allele (4). While we found that all the mice transplanted with homozygous mutant cells developed a myeloproliferative syndrome similar to JMML, only a subset of these genetically identical reconstituted mice went on to develop more acute disease. These results suggested that additional somatic ge-

* Corresponding author. Mailing address: Department of Molecular Genetics and Microbiology, P.O. Box 100266, University of Florida College of Medicine, Gainesville, FL 32610. Phone: (352) 392-3296. Fax: (352) 392-3133. E-mail: brannan@mgm.ufl.edu.

netic mutations are required for disease progression in mice and humans.

To identify somatic mutations that cooperate with the loss of *Nf1* to cause progression to acute leukemia, we have crossed the $Nf1^{Fcr}$ allele onto the BXH-2 mouse genetic background. BXH-2 mice express an ecotropic murine leukemia virus (MuLV) passed from mother to offspring by infection in utero (3). By 1 year of age, nearly 100% of these viremic BXH-2 mice develop an AML that is very similar to AML in humans (28). Previous analysis of BXH-2 tumors has shown that they are nearly all monoclonal in origin and contain one or more somatically acquired MuLV integrations (2). Several investigators have used the BXH-2 system to identify genes that are causally associated with the development of murine myeloid disease by cloning chromosomal sites from tumor DNA into which the MuLV has integrated (6, 16, 23, 25, 26). In many of these cases, specific regions were found to harbor proviral insertions in multiple tumors, each derived from independent mice. Therefore, the identification of a common site of viral integration has served as a good indicator that the region harbors a gene that, when mutated by proviral insertion, contributes to the development of myeloid leukemia. While most of the common sites of viral integration identified in BXH-2 mice are thought to activate the expression of dominant proto-oncogenes (16, 23, 25, 26), one notable exception has been the identification of a common site of viral integration which inactivates the tumor suppressor gene, *Nf1*. This common site of viral integration, named *Evi2* (ectotropic viral integration 2), was identified in 10 to 15% of BXH-2 tumors and found to be within a large intron of the *Nf1* gene (6, 8). Using BXH-2 tumors in which biallelic *Evi2* integrations had occurred, it was shown that the presence of the virus resulted in premature truncation of the *Nf1* transcript, such that no full-length product could be produced (6, 21).

Because loss of *Nf1* expression has been shown to be a mechanism of myeloid tumorigenesis in BXH-2 mice, we have exploited this system as a means to identify cooperating events in the progression of JMML. Our strategy has been to backcross C57BL/6J mice containing the $Nf1^{Fcr}$ mutation onto the BXH-2 genetic background for three generations, then age the resulting $Nf1^{Fcr}$ heterozygous N3 mice until they develop acute leukemia, and subsequently collect tumors from each animal. In this manner, we have established a panel of tumors derived from 66 independent N3 BXH-2 $Nf1^{Fcr/+}$ animals. By cloning sites of viral integration from individual tumors in the panel, we have identified a major common site of viral integration, *Epi1*, occurring in 44% of tumors in the panel. Interestingly, we also found that *Epi1* is affected at nearly the same frequency in BXH-2 tumors without an *Nf1* mutation. This indicates *Epi1* represents the most common site of somatic viral integration identified to date in BXH-2 mice.

MATERIALS AND METHODS

Mice and harvesting of tumor tissue. All animal studies were performed according to federal guidelines and University of Florida institutional policies. Mice were aged up to 8 months. When a mouse became moribund it was sacrificed and a necropsy was performed. The necropsy included the following: a physical characterization of the mouse; determination of lymph nodes, spleen, and liver relative size; and liver, spleen, bone marrow, and lymph node fixation in 10% neutral buffered formalin with subsequent embedding in paraffin, sectioning, and staining with hematoxylin and eosin (H&E). Tissue was also frozen in liquid nitrogen to make RNA or DNA. Finally, four lymph nodes were perfused with media, and half of the resulting cells were used to make DNA and half were used to make frozen aliquots of viable cells.

DNA and RNA preparation. DNA was made from brain and lymph node to use for molecular characterization of the tumors. Tissue (0.4 g) was lysed in homogenizing solution (1× SSC [1× SSC is 150 mM sodium chloride, 15 mM sodium citrate, 0.02 mM citric acid], 1% sodium dodecyl sulfate [SDS], and pronase E [0.25 mg/ml; Sigma]). Samples were vortexed well to mix, and were incubated at 37°C for 1 h and vortexed every 15 min during the incubation. The samples were then extracted once each with phenol (U.S. Biochemical) and phenol-chloroform-isoamyl alcohol (50:49:1; Fisher Scientific). The DNA was precipitated and resuspended in 9 ml of 1× SSC. To this, 0.5 ml of RNase A (2 mg/ml; Sigma) was added and incubated at 37°C for 30 min; this was followed by the addition of 0.5 ml of pronase E (5 mg/ml), and the mixture was then incubated at 37°C for 30 min. The DNA was then extracted again as above and precipitated in ethanol. RNA was made according to the protocol provided with RNAzol B (Tel-Test, Inc.).

Southern and Northern blots. Five micrograms of genomic DNA was digested with the appropriate restriction enzyme in a total volume of 40 μl at 37°C (or appropriate temperature) for at least 4 h. After 4 h 20 more units of enzyme was added and incubated for 2 more hours at 37°C. The digests were electrophoresed on a 0.8% agarose TPE gel (90 mM Tris-HCl, 26 mM phosphoric acid, 2 mM EDTA). The gel was then soaked in denaturing solution (1.48 M sodium chloride, 0.5 M sodium hydroxide) for 45 min with gentle shaking. The gel was then transferred to neutralizing solution (1 M Tris-HCl, 3 M sodium chloride, 0.2 M hydrochloric acid) and soaked for 1.5 h with gentle shaking. The gel was then blotted onto Hybond (Amersham) membrane in 10× SSC overnight. The membrane was then baked for 2 h at 80°C.

Ten micrograms of total RNA was run on the gel for Northern blots. The 1% agarose gel was made in 1× MOPS [20 mM 3-(*N*-morpholino)propanesulfonic acid, 5 mM sodium acetate, 1 mM EDTA] and 18% formaldehyde. The RNA samples were mixed with 16 μl of sample buffer (300 μl of formamide, 105 μl of formaldehyde, 60 μl of 10× MOPS, 60 μl of 10% bromophenol blue, and 3 μl of ethidium bromide [10 mg/ml]) and incubated at 65°C for 5 min and then put on ice until loaded. After electrophoresis, the RNA was then transferred to Hybond membrane by blotting overnight in 10× SSC. The membrane was then baked for 2 h at 80°C.

The [α-^{32}P]dCTP-labeled, random-primed probes were made using a random priming kit (Stratagene). The nick-translated probes were labeled using a nick translation kit (Amersham). The *Nf1* probe for detecting LOH was hybridized as previously described (4). All other probes were hybridized according to the Church and Gilbert method (9). The membranes were hybridized for 2 h at 65°C, and then 5 ml of fresh hybridization buffer was added. The denatured probes were added, and the membranes were hybridized overnight at 65°C. The next day the membranes were washed at 65°C in 0.2× SSCP and 0.1% SDS (9). The membranes were then subjected to autoradiography.

Cloning flanking DNA. *Bam*HI-restricted tumor DNA was size fractionated on a sucrose gradient. Then, the fraction with the viral integration was identified and a phage library was made using that fraction. The library was screened to isolate the viral-cellular DNA junction fragment. Specifically, the sucrose gradient was prepared by placing 11.5 ml of 25% sucrose in STE buffer (10 mM Tris, 6 mM EDTA, 10 mM NaCl) in polyallomer tubes (Beckman) and freeze-thawing the solution twice. Fifty micrograms of tumor DNA was digested with *Bam*HI in a volume of 300 μl for about 2 h, and then more enzyme was added and the DNA was digested for another 2 h. The DNA was then extracted twice by the phenol–phenol-chloroform-isoamyl alcohol method and ethanol precipitated. The DNA was washed with 70% ethanol, dried, and then was resuspended in 110 μl of STE buffer. The DNA was layered on the sucrose gradient and spun at 30,000 rpm at 20°C overnight using an SW41Ti rotor (Beckman). Fractions (0.5 ml) were collected from the gradient, and 60 μl was saved to run on a gel as a control. Ethanol (100%) was added to the rest of the fraction and stored at −20°C. The 60-μl aliquots from the fractions were run on a 0.8% TPE gel along with the unfractionated DNA. The gel was blotted and probed with pAKV5 (17) to determine which fraction had the viral integration. *Bam*HI restricted genomic DNA from the positive fraction was then ligated into the Lambda DASH II vector (Stratagene), and the resulting Gigapack III Gold packaged (Stratagene) phage library was screened according to the manufacturer's instructions using the pAKV5 (17) viral probe. Once plaque-pure phage was obtained, phage DNA was prepared and the insert was subcloned into pBluescript KS(+) (Stratagene).

Interspecific backcross mapping. Interspecific backcross progeny were generated by mating (C57BL/6J × *Mus spretus*)F_1 females and C57BL/6J males as described (11). A total of 205 N_2 mice were used to map the *Epi1* locus (see text for details). DNA isolation, restriction enzyme digestion, agarose gel electro-

phoresis, Southern blot transfer and hybridization were performed essentially as described previously (17a). All blots were prepared with Hybond-N^+ nylon membrane (Amersham). The probe, a 1.3-kb *Bam*HI/*Pst*I fragment of mouse genomic DNA, was labeled with [α-^{32}P]dCTP using a random-primed labeling kit (Stratagene); washing was done to a final stringency of 1.0× SSCP and 0.1% SDS at 65°C. A fragment of 10.5 kb was detected in *Bam*HI-digested C57BL/6J DNA, and a fragment of 7.8 kb was detected in *Bam*HI-digested *M. spretus* DNA. The presence or absence of the 7.8-kb *Bam*HI *M. spretus*-specific fragment was monitored in backcross mice. A description of the probes and restriction fragment length polymorphisms for the loci linked to *Epi1*, including *Estra, Myb,* and *Tcf21*, has been reported previously (29). Recombination distances were calculated using Map Manager, version 2.6.5. Gene order was determined by minimizing the number of recombination events required to explain the allele distribution patterns.

Immunophenotyping of leukemias. Cryopreserved leukemic cells harvested from enlarged lymph nodes were thawed and washed twice in phosphate-buffered saline with 2% heat-inactivated fetal bovine serum (wash buffer). Single cell suspensions were incubated with antibodies directly conjugated to fluorochromes for 20 to 30 min on ice, washed, and resuspended in wash buffer. Analysis was carried out using a FACScan flow cytometer. A total of 10,000 events were collected on each sample, and results were analyzed using Cell Quest Software (Becton Dickinson). All antibody combinations included anti-CD45-TRI-COLOR. Other antibodies used in combination were anti-Ly-6G(Gr-1)-fluorescein isothiocyanate (FITC) and anti-CD11b(Mac-1)-phycoerythrin (PE), anti-CD59-FITC and anti-CD31-PE, anti-CD34-FITC and anti-CD117(c-kit)-PE, anti-CD45R(B220)-FITC and anti-CD19-PE, anti-CD90.2(Thy1.2)-FITC and anti-CD3-PE, anti-CD41-FITC and anti-CD61-PE, and anti-CD86-FITC and anti-Ly-71(F4/80)-PE. The dominant leukemic cell population was gated using forward scatter, side scatter, and CD45. Expression of antigens on the leukemic cells was assessed relative to isotype controls. Cytospins were also prepared from thawed cells and stained with Wright's Giemsa stain prior to morphological examination. Maturation of cells was assessed by the method of Brecher et al. (5).

RESULTS

Development and characterization of the tumor panel. We placed the *Nf1^{Fcr}* mutation on the BXH-2 genetic background by backcrossing for three generations. All N3 mice tested were found to be viremic (data not shown). We aged *Nf1^{Fcr}* heterozygous N3 mice until they became moribund due to the development of AML and then collected tumor material from each animal. In an initial pilot study, in which we aged both *Nf1^{Fcr}* heterozygous N3 mice and their wild-type control littermates, we found that the *Nf1^{Fcr}* heterozygous mice developed AML at a significantly higher rate than controls: 50% of heterozygous mice required sacrifice at 5.5 months versus 8.5 months for controls ($P = 0.003$ using the rank sum test). This indicated that BXH-2 mice containing one mutant *Nf1^{Fcr}* allele exhibited a decreased latency for myeloid disease. Based on these data, we initiated a larger aging study using only heterozygous mice and accumulated a panel of tumors isolated from a total of 66 independent heterozygous *Nf1^{Fcr}* N3 mice. Using Southern blot analysis, we determined that 89% of the tumors in the panel have sustained a second genetic hit to the *Nf1* locus, either by LOH or by *Evi2* integration. Furthermore, we found that all the tumors from heterozygous *Nf1^{Fcr}* N3 mice had at least one somatically acquired viral integration. Even tumors which sustained a viral integration at *Evi2* contained at least one additional somatic viral integration. This indicates that loss of *Nf1* on the BXH-2 background alone is not sufficient to induce acute myeloid disease, but the additional somatic mutations are necessary for tumor progression to AML.

Identification of a common site of viral integration, *Epi1*. To identify potential cooperating genes for myeloid tumor progression, we cloned genomic DNA flanking sites of somatic viral integration from individual tumors in the panel. Using the ecotropic retroviral probe pAKV5 (17), we isolated a unique *Bam*HI restriction fragment from tumor DNA isolated from animal 355. After isolation of a nonrepetitive probe from the cloned fragment, dubbed probe E, we screened the entire panel of tumors for rearrangements by Southern blot. Not only were we able to confirm a rearrangement in the original tumor (data not shown), but we also detected rearrangements in many additional tumor DNA samples (Fig. 1A). This indicated that we had identified a common site of viral integration, which we designated *Epi1* for ecotropic proviral integration site 1.

The mouse chromosomal location of *Epi1* was determined by interspecific backcross analysis using progeny derived from matings of [(C57BL/6J × *M. spretus*)F_1 × C57BL/6J] mice. This interspecific backcross mapping panel has been typed for over 3,000 loci that are well distributed among all the autosomes as well as the X chromosome (11). C57BL/6J and *M. spretus* DNAs were digested with several enzymes and analyzed by Southern blot hybridization to obtain informative restriction fragment length polymorphisms using a mouse *Epi1* genomic DNA probe. The 7.8-kb *Bam*HI *M. spretus* restriction fragment length polymorphism (see Materials and Methods) was used to follow the segregation of the *Epi*1 locus in backcross mice. The mapping results indicated that *Epi1* is located in the proximal region of mouse chromosome 10 linked to *Estra*, *Myb*, and *Tcf21*. Although 128 mice were analyzed for every marker and are shown in the segregation analysis (Fig. 2), up to 181 mice were typed for some pairs of markers. Each locus was analyzed in pairwise combinations for recombination frequencies using the additional data. The total number of mice exhibiting recombinant chromosomes and the total number of mice analyzed for each pair of loci are as follows (listed in the most likely gene order): centromere-*Estra*, 9 of 181; *Myb*, 0 of 161; *Epi1*, 1 of 142; *Tcf21*. The recombination frequencies (expressed as genetic distances ± standard error [in centimorgans]) are as follows: *Estra*, 5.0 ± 1.6; *Myb* and *Epi1*, 0.7 ± 0.7; *Tcf21*. No recombinants were detected between *Myb* and *Epi1* in 161 animals typed in common, suggesting that the two loci are within 1.9 cM of each other (upper 95% confidence limit).

Epi1 maps 3′ of the *Myb* locus. Based on the lack of genetic recombination observed between *Epi1* and *Myb*, we sought to determine if these two loci were physically linked. We isolated a bacterial artificial chromosome clone (529J1 BAC; Research Genetics) using the original *Epi1* probe (Fig. 1B, probe E) and determined that the *Myb* gene was also contained on this same BAC clone. We used this BAC clone to generate a restriction map of the *Epi1* region and to isolate additional probes (Fig. 1B, probes A, B, D, and F). Using these new probes, as well as the previously isolated *Ahi1* probe (18) (referred to here as probe C), we determined that a total of 29 tumors, or 44% of the panel, contained a somatic *Epi1* rearrangement (Table 1). While no rearrangements were detected with probe A, the majority of rearrangements were detected by probes B and C (indicating an insertion into the 11-kb *Bam*HI fragment) or by probes D and E (indicating an insertion into the 13.5-kb *Bam*HI fragment). Rearrangements were detected with probe F in four tumors. These data indicate that most of the viral insertions have occurred 30 to 40 kb downstream of the last exon of *Myb*.

Based on the location of these somatic insertions, it seemed possible that the integrated proviruses affect *Myb*. However, all

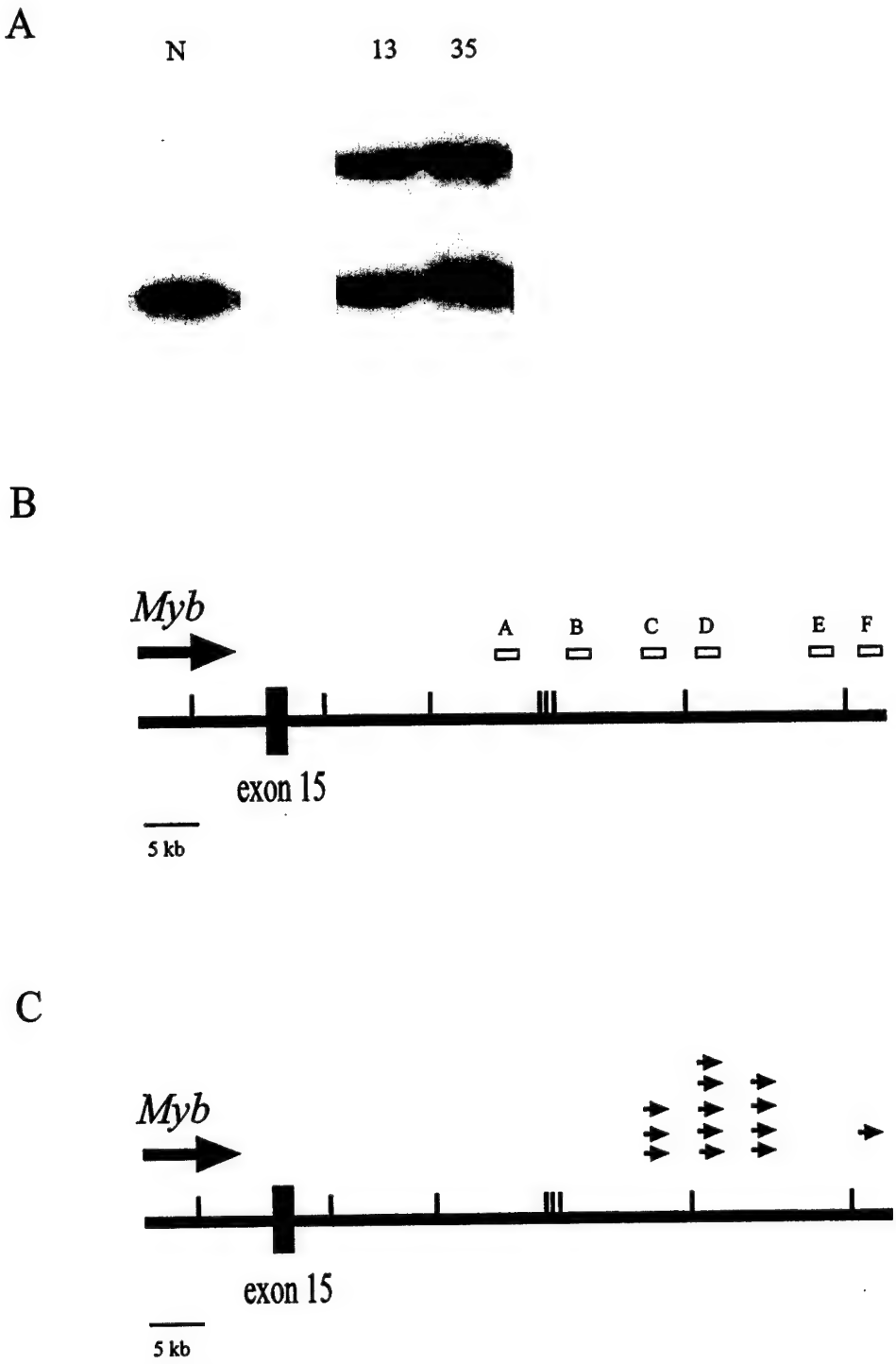

FIG. 1. The *Epi1* locus. (A) Southern blot analysis showing rearrangements of the *Epi1* locus in two independent tumors. Normal DNA (N) and tumor DNAs were digested with *Bgl*II and hybridized with probe C from the *Epi1* locus. (B) Map of the *Epi1* region relative to the *Myb* gene. The large line represents the region 3′ of the *Myb* gene. The small hash marks represent *Bam*HI sites in the region, the large box is exon 15 of the *Myb* gene, the large arrow shows the direction of transcription of *Myb*, and the small boxes above the line are the probes isolated from the region. Probe C is the *Ahi1* probe (18). (C) Location and orientation of 13 proviruses integrated in *Epi1* relative to the *Myb* gene. The small arrows above the line show the location and orientation of the viral integrations in the *Epi1* locus.

previously reported viral insertions proven to affect *Myb* occur within the *Myb* gene. For example, viral integration in the 5′ end has been shown to result in overexpression of a virally promoted chimeric mRNA that lacks the three 5′-most *Myb* coding exons (36). In addition, integrations in the 3′ end of *Myb* have been shown to result in the production of a Myb protein that is stabilized due to truncation of the carboxy terminus (36). Therefore, we rescreened our panel using a

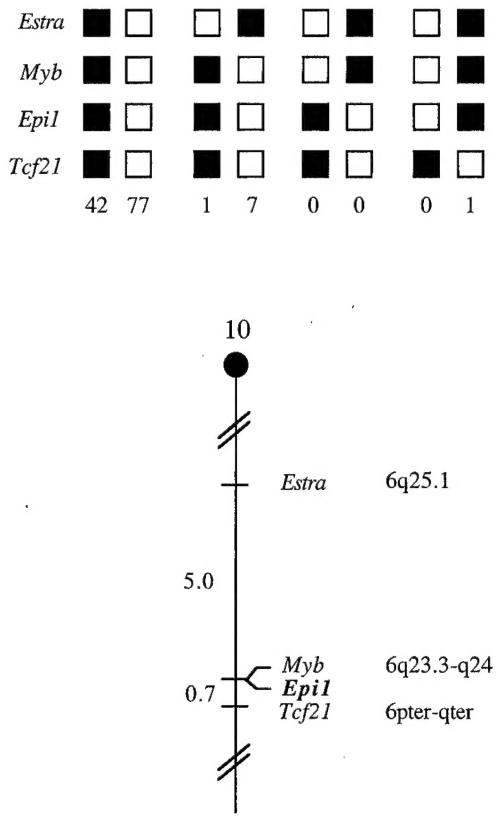

FIG. 2. Epi1 maps in the proximal region of mouse chromosome 10. *Epi1* was placed on mouse chromosome 10 by interspecific backcross analysis. The segregation patterns of *Epi1* and flanking genes in 128 backcross animals that were typed for all loci are shown at the top of the figure. For individual pairs of loci, more than 128 animals were typed (see text). Each column represents the chromosome identified in the backcross progeny that was inherited from the (C57BL/6J × *M. spretus*)F_1 parent. The black boxes represent the presence of a C57BL/6J allele, and white boxes represent the presence of a *M. spretus* allele. The number of offspring inheriting each type of chromosome is listed at the bottom of each column. A partial chromosome 10 linkage map showing the location of *Epi1* in relation to linked genes is shown at the bottom of the figure. Recombination distances between loci in centimorgans are shown to the left of the chromosome, and the positions of loci in human chromosomes, where known, are shown to the right. References for the human map positions of loci cited in this study can be obtained from the Genome Data Base, a computerized database of human linkage information maintained by The William H. Welch Medical Library of The Johns Hopkins University (Baltimore, Md.).

series of *Myb* probes, but we found only two tumors that contained insertions within the *Myb* gene.

To ascertain if viral integrations at *Epi1* affect *Myb*, we determined the orientation of the integrated provirus in 13 of the tumors in which we were able to confirm the presence of a full-length virus. We found that in all 13 cases, the virus had integrated in the same transcriptional orientation as *Myb* (Fig. 1C). These data are consistent with a mechanism of viral enhancement in which the viral enhancer located in the 5′ long terminal repeat serves to activate transcription of an upstream gene (19). With this in mind, we assayed the level of *Myb* expression in the tumors by Northern blotting of total RNA isolated from several tumors with and without a viral integration at *Epi1*. We found that *Myb* was expressed in tumors

TABLE 1. Tumors derived from N3 BXH-2 $Nf1^{Fcr/+}$ mice with *Epi1* insertions[a]

Tumor no.	*Nf1* status	No. of somatic proviruses	*Epi1* probe(s) detecting *Bam*HI rearrangement
10	*Evi2*	3	D, E
11	$Nf1^{Fcr}$/+	1	D, E
13	LOH	3	D, E
14	*Evi2*	2	B, C
33	LOH	3	B, C
35	LOH	5	D, E
46	*Evi2*	2	F
56	LOH	2	D, E
84	LOH	2	B, C
103	LOH	2	D, E
355	LOH	1	D, E
356	*Evi2*	3	D, E
358	LOH	2	F
368	LOH	5	D, E
371	LOH	1	D, E
419	LOH	2	D, E
468	LOH	2	B, C
522	LOH	5	D, E
570	LOH	2	D, E
603	$Nf1^{Fcr}$/+	1	D, E
639	*Evi2*	2	F
647	LOH	2	F
660	*Evi2*	3	D, E
662	LOH	3	B, C
665	*Evi2*	3	B, C
671	LOH	2	B, C
675	$Nf1^{Fcr}$/+	2	D, E
725	*Evi2*	1	D, E
1858	*Evi2*	1	F

[a] "Tumor no." refers to the pedigee number of the animal from which the tumor was derived. "*Nf1* status" refers to the status of the *Nf1* allele in the tumor; all the mice began as heterozygous for the *Nf1* mutation ($Nf1^{Fcr/+}$), but many of the tumors lost the remaining wild-type allele (LOH) or suffered a proviral integration in the *Nf1* gene (*Evi2*). "No. of somatic proviruses" refers to the number of somatically acquired proviral integrations detected in the tumor DNA. "*Epi1* probe(s) detecting *Bam*HI rearrangement" indicates the probe(s) from Fig. 1 which detects the somatic rearrangement in the *Epi1* locus in the particular tumor.

whether or not the tumors harbored *Epi1* integrations. Of note, expression levels were not increased in tumors containing an *Epi1* insertion relative to expression levels in tumors lacking such a viral insertion (Fig. 3). However, tumors lacking *Epi1* insertions may have upregulated *Myb* by another mechanism. In any case, these data show that the *Myb* gene is indeed expressed in the *Epi1* tumors, but that a viral insertion at *Epi1* does not appear to result in marked overexpression of *Myb*.

Phenotype of *Epi1* tumors. We performed histological analysis of H&E stained tissue sections from a subset of the animals listed in Table 1 (tumors 355, 419, 468, 660, and 671). This analysis revealed that while there was a modest variation in the morphology of the leukemic cells, the overall pattern was similar. Common features included the presence of leukemic cells at the young-intermediate stages of myeloid differentiation accompanied by numerous pseudo-Gaucher cells (indicative of high cell turnover); lymph nodes that were effaced by the leukemia; spleens that exhibited modest areas of residual white pulp but massive expansion of the red pulp predominantly by leukemic cells, but with some admixed megakaryocytes and erythroid precursors; livers that showed leukemic infiltrates with marked accumulations in the periportal areas and with

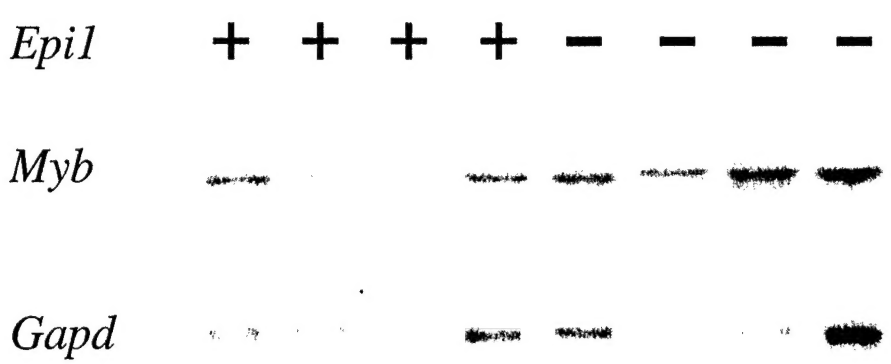

FIG. 3. Northern blot analysis of *Myb* expression in *Epi1* and non-*Epi1* tumors. RNA derived from four tumors containing somatic viral insertion at *Epi1* (+) and four tumors without this viral insertion (−) were analyzed by Northern blotting. The top panel shows the hybridization with a *Myb* cDNA probe, and the bottom panel shows the same blot stripped and rehybridized with a control probe for *Gapd*.

infiltration into the parenchyma and/or sinusoids; and bone marrows filled with leukemic cells (accompanied by pseudo-Gaucher histiocytes) (Fig. 4A to C).

Finally, analysis on viable isolates of these same five tumors (tumors 355, 419, 468, 660, and 671; Table 1) revealed that all five were relatively uniform: almost entirely young forms (blasts) by morphology (Fig. 4D) that express an immunophenotype consistent with granulocyte/monocyte precursors [Ly-6G(Gr-1)+, CD11b(Mac-1)variable, CD31$^+$, CD59$^+$, CD117(c-kit)variable, CD34lo, Ly-71(F4/80)lo] (Fig. 5). That the tumor cells had only a weak CD45R (B220) signal and were clearly CD19 negative strongly suggests that the cells are not B-lymphoid cells. In addition, the T-cell markers CD90.2 and CD3 were either negative or weak, indicating the cells are not T lymphocytes. These tumors as well as several others were confirmed to be of myeloid origin as they were found to express the myeloid cell markers c-*fms* and myeloperoxidase by Northern blot analysis. In further support of this origin, we detected no rearrangements of the T-cell receptor genes or the immunoglobulin heavy chain gene. These data indicate that the mice had developed myeloid leukemias and show that the five tumors examined in detail were relatively homogeneous in character. These five leukemias all contained *Epi1* insertions and lacked *Nf1*. Their common characteristics likely reflect their common genetic pathogenesis: it contrasts with the phenotypic heterogeneity we have observed in unselected, genetically heterogeneous, BXH-2 leukemias (S. Kogan, unpublished observations).

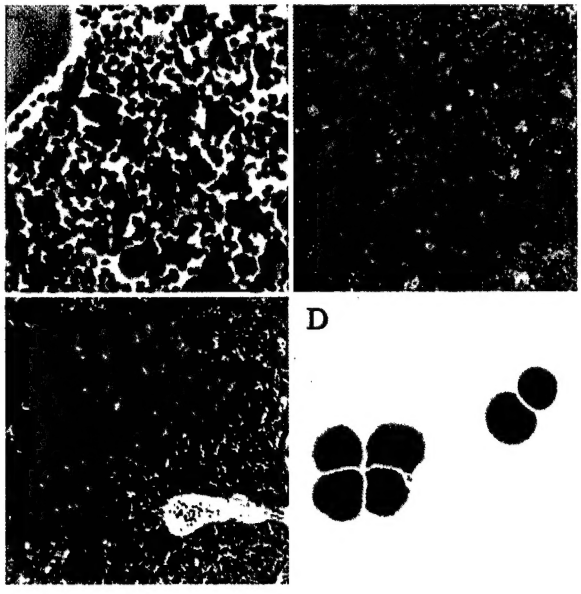

FIG. 4. Leukemia morphology. (A) Bone marrow histology showing immature cells and numerous pseudo-Gaucher histiocytes. Magnification, ×250. (B) Spleen histology showing expanded red pulp with leukemic cells accompanied by large megakaryocytes and few small dark-staining erythroid precursors. Residual white pulp is visible at lower right. Magnification, ×100. (C) Liver histology showing massive infiltration of leukemic cells. Magnification, ×100. H&E stain was used for panels A to C. (D) Cytology (Wright's Giemsa stain) of leukemic cells prepared from lymph node. Magnification, ×500.

Analysis of wild-type BXH-2 tumors. Finally, to determine if viral integrations at *Epi1* were restricted to tumors containing mutations at the *Nf1* locus, we analyzed a set of BXH-2 tumors that were wild-type at the *Nf1* locus, as well as a set of tumors that has suffered one somatic viral integration within *Nf1* (*Evi2*). We found that in both groups of 23 tumors, 10 tumors (43%) exhibited a viral integration in *Epi1*. Interestingly, however, we found that the distribution of proviral insertions in *Epi1* was different between the two groups. Proviral insertions occurred in a discrete region in the tumors with wild-type *Nf1*, with rearrangements being detected only by probes D and E (Fig. 1B). In contrast, tumors harboring an *Evi2* insertion showed a much broader region of proviral insertions in *Epi1*, with rearrangements being detected by probes B and C, D and E, or F. This difference in distribution of proviral insertions between the two genotypic groups may reflect the differentiation state of the cell at the time of viral infection. For example, myeloid cells with only one intact copy of *Nf1* may display a more open chromatin conformation at *Epi1* and hence present a wider target area for viral integration than cells with both copies intact. Regardless of the slight difference in the specific region of integration, these data demonstrate that *Epi1* represents a major site of viral integration in approximately 43% of all BXH-2 myeloid tumors.

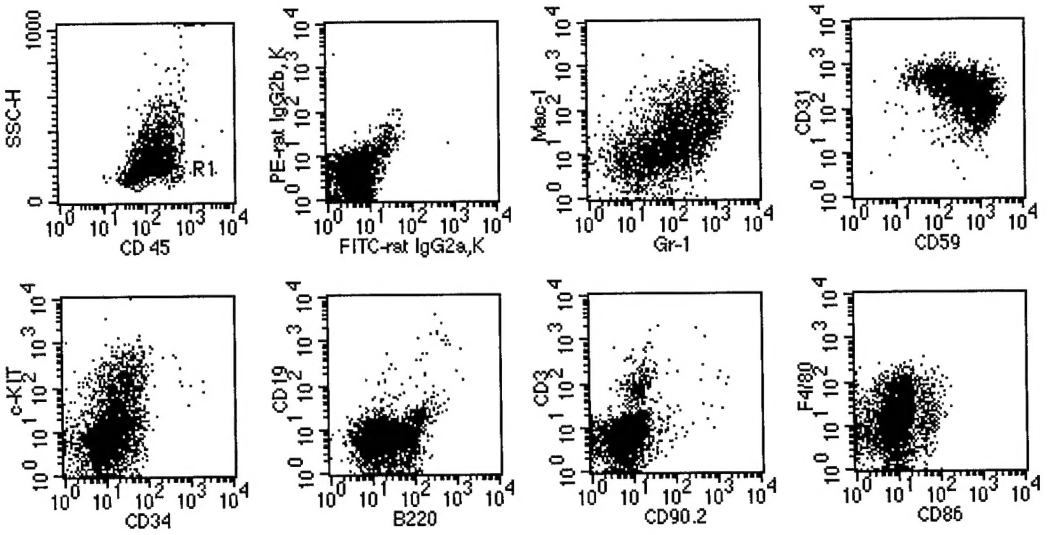

FIG. 5. Flow cytometric analysis of a representative leukemia. Data in panel CD45/SSC are ungated; for those in the remaining panels, the gate was set at R1.

DISCUSSION

We have previously shown that loss of *Nf1* in the hematopoietic lineage causes a myeloproliferative syndrome similar to JMML (22). However, we found that only a subset of all of these reconstituted mice went on to develop more acute disease, suggesting that additional somatic genetic mutations are required for disease progression in mice and humans. To identify candidate genes that may cooperate with the loss of the *Nf1* gene in progression of myeloid leukemia, we have established a panel of tumors derived from 66 independent N3 BXH-2 $Nf1^{Fcr/+}$ animals. We have determined that 89% of the tumors in the panel have sustained a second genetic hit to the *Nf1* locus, either by LOH or by viral integration within the *Nf1* locus (*Evi2*), demonstrating that the vast majority of the tumors developed in a pathway involving *Nf1* gene loss. Therefore, through the introduction of one mutant *Nf1* allele, we have obtained a sixfold higher frequency of *Nf1*-dependent myeloid leukemia compared to the parental BXH-2 strain.

Analysis of the panel revealed that these tumors harbored a mean of three somatically acquired viral insertions. By cloning these sites of viral integration from individual tumors in the panel, we were able to identify a common site of viral integration, *Epi1*, occurring in 44% of tumors in the panel. The *Epi1* locus was found to map 30 to 40 kb downstream of the last exon of the *Myb* gene. Interestingly, this site has previously been implicated in B-cell lymphoma: Jiang et al. reported that infection of newborn mice with a combination of Abelson MuLV (contains the v-*abl* oncogene) and Moloney MuLV (the insertional mutagen) resulted in B-cell lymphoma (18). They determined that 16% of these tumors had Moloney MuLV insertions at the *Ahi1* locus, located approximately 30 kb 3′ of the last exon of *Myb*. Again, similar to our findings, they determined that these viral integrations did not result in overexpression of *Myb*. Based on this result, Jiang et al. concluded that the viral insertions activated an as-yet-unidentified gene. However, one alternate interpretation of these data is that these downstream viral integrations do affect *Myb* expression, but not by upregulating transcription. Instead, the virus may simply prevent the downregulation of *Myb* that normally occurs during myeloid differentiation. In fact, it is well known that either constitutive expression of full-length *Myb* or truncated *Myb* can block differentiation of leukemic cell lines (10, 12, 24, 30, 35, 37). Furthermore, downregulation of *Myb* is known to be essential for terminal differentiation of the myeloid and B-cell lineages (27). Therefore, it is possible that constitutive expression of *Myb* in combination with v-*abl* induces B-cell lymphoma, whereas constitutive expression of *Myb* in combination with the loss of *Nf1* function leads to AML. Alternatively, it is possible that viral integration into this locus affects a gene other than *Myb*. In fact, it is possible that viral integration in B-cells affects one gene (the *Ahi1* gene), but viral insertion in myeloid cells affects a different gene (the *Epi1* gene). In any case, whether viral insertions in *Epi1* affect *Myb* or another gene, we have provided very good evidence that *Epi1* does play an important role in BXH-2 myeloid leukemia. The finding that approximately 43% of BXH-2 tumors harbor viral insertion in *Epi1* indicates that *Epi1* may represent the most common site of viral integration in BXH-2.

Because proviral integrations in *Epi1* are so common in BXH-2 tumors, one might be tempted to conclude that this event alone is sufficient to cause AML. However, data obtained from our N3 BXH-2 $Nf1^{Fcr/+}$ tumors suggest that additional cooperating mutations are required for progression to AML: 27 out of 29 of these tumors have another obvious somatic mutation in addition to a proviral insertion in *Epi1*. Furthermore, we can conclude that at least in these tumors, the cooperating mutation is the loss of the *Nf1* gene since 26 out of these 29 tumors (90%) with viral integrations at *Epi1* also exhibit loss of *Nf1* function. But loss of *Nf1* is clearly not the only possible cooperating mutation since *Nf1* is mutated in only 10 to 15% of BXH-2 tumors. Therefore, other genes must be able to serve as a cooperating gene for *Epi1*-associated AML. Since *Nf1* is known to affect the Ras pathway, it is tempting to speculate that these other genes might be involved in this same pathway.

Finally, it is unclear whether the loss of *Nf1* plus a proviral

insertion at *Epi1* is sufficient to cause AML. Among our panel of tumors, five appear to have the *Epi1* integration as the only other somatic mutation (Table 1, tumors 14, 46, 355, 371, and 639), suggesting that loss of *Nf1* plus insertion at *Epi1* is acutely leukemogenic. However, it is possible that these five tumors harbor other somatic mutations that we are unable to detect. Further studies of BXH-2 and *Nf1* murine models of myeloid neoplasms should allow the combinations of events sufficient for leukemogenesis to be definitively assessed.

ACKNOWLEDGMENTS

We thank Michael Elmore and Deborah B. Householder for excellent technical assistance. We thank Linda Wolff for *Myb* probes and Paul Jolicoeur for the *Ahi1* probe (Probe C, Fig. 1B).

This research was supported by a grant from the Department of Defense, U.S. Army Medical Research and Materiel Command (DAMD17-97-1-7339), to C.I.B.; by grants from the NIH/NCI (CA75986 and CA84221) to S.C.K.; by a Leukemia Research Fund grant to D.A.L.; and, in part, by the National Cancer Institute, DHHS. S.C.K. is a recipient of a Burroughs Wellcome Fund Career Award and is an Edward Mallinckrodt Jr. Foundation Scholar.

REFERENCES

1. **Bader, J. L., and R. W. Miller.** 1978. Neurofibromatosis and childhood leukemia. J. Pediatr. **92:**925–929.
2. **Bedigian, H. G., D. A. Johnson, N. A. Jenkins, N. G. Copeland, and R. Evans.** 1984. Spontaneous and induced leukemias of myeloid origin in recombinant inbred BXH mice. J. Virol. **51:**586–594.
3. **Bedigian, H. G., L. A. Shepel, and P. C. Hoppe.** 1993. Transplacental transmission of a leukemogenic murine leukemia virus. J. Virol. **67:**6105–6109.
4. **Brannan, C. I., A. S. Perkins, K. S. Vogel, N. Ratner, M. L. Nordlund, S. W. Reid, A. M. Buchberg, N. A. Jenkins, L. F. Parada, and N. G. Copeland.** 1994. Targeted disruption of the neurofibromatosis type-1 gene leads to developmental abnormalities in heart and various neural crest-derived tissues. Genes Dev. **8:**1019–1029.
5. **Brecher, G., K. Endicott, H. Gump, and H. P. Brawner.** 1948. Effects of X-ray on lymphoid and hemopoietic tissues of albino mice. Blood **3:**1259–1274.
6. **Buchberg, A. M., H. G. Bedigian, N. A. Jenkins, and N. G. Copeland.** 1990. *Evi-2*, a common integration site involved in murine myeloid leukemogenesis. Mol. Cell. Biol. **10:**4658–4666.
7. **Castro-Malaspina, H., G. Schaison, S. Passe, A. Pasquier, R. Berger, C. Bayle-Weisgerber, D. Miller, M. Seligman, and J. Bernard.** 1984. Subacute and chronic myelomonocytic leukemia in children (juvenile CML). Cancer **54:**675–686.
8. **Cawthon, R. M., L. B. Andersen, A. M. Buchberg, G. F. Xu, P. O'Connell, D. Viskochil, R. B. Weiss, M. R. Wallace, D. A. Marchuk, M. Culver, et al.** 1991. cDNA sequence and genomic structure of EV12B, a gene lying within an intron of the neurofibromatosis type 1 gene. Genomics **9:**446–460.
9. **Church, G. M., and W. Gilbert.** 1985. The genomic sequencing technique. Prog. Clin. Biol. Res. **177:**17–21.
10. **Clarke, M. F., J. F. Kukowska-Latallo, E. Westin, M. Smith, and E. V. Prochownik.** 1988. Constitutive expression of a c-*myb* cDNA blocks Friend murine erythroleukemia cell differentiation. Mol. Cell. Biol. **8:**884–892.
11. **Copeland, N. G., and N. A. Jenkins.** 1991. Development and applications of a molecular genetic linkage map of the mouse genome. Trends Genet. **7:**113–118.
12. **Cuddihy, A. E., L. A. Brents, N. Aziz, T. P. Bender, and W. M. Kuehl.** 1993. Only the DNA binding and transactivation domains of c-Myb are required to block terminal differentiation of murine erythroleukemia cells. Mol. Cell. Biol. **13:**3505–3513.
13. **De Bella, K., J. Szudek, and J. M. Freidman.** 2000. Use of National Institutes of Health criteria for diagnosis of neurofibromatosis 1 in children. Pediatrics **105:**608–614.
14. **Gadner, H., and O. A. Haas.** 1992. Experience in pediatric myelodysplastic syndromes, vol. 6. W. B. Saunders Company, Philadelphia, Pa.
15. **Gutmann, D. H., and F. S. Collins.** 1993. The neurofibromatosis type 1 gene and its protein product, neurofibromin. Neuron **10:**335–343.
16. **Hansen, G. M., D. Skapura, and M. J. Justice.** 2000. Genetic profile of insertion mutations in mouse leukemias and lymphomas. Genome Res. **10:**237–243.
17. **Herr, W., and W. Gilbert.** 1983. Somatically acquired recombinant murine leukemia proviruses in thymic leukemias of AKR/J mice. J. Virol. **46:**70–82.
17a. **Jenkins, N. A., N. G. Copeland, and B. K. Lee.** 1982. Organization, distribution, and stability of endogenous ecotropic murine leukemia virus DNA sequences in chromosomes of *Mus musculus*. J. Virol. **43:**26–36.
18. **Jiang, X., L. Villeneuve, C. Turmel, C. A. Kozack, and P. Jolicoeur.** 1994. The *Myb* and *Ahi-1* genes are physically very closely linked on mouse chromosome 10. Mamm. Genome **5:**142–148.
19. **Jonkers, J., and A. Berns.** 1996. Retroviral insertional mutagenesis as a strategy to identify cancer genes. Biochim. Biophys. Acta **1287:**29–57.
20. **Kalra, R., D. C. Paderanga, K. Olson, and K. M. Shannon.** 1994. Genetic analysis is consistent with the hypothesis that NF1 limits myeloid cell growth through p21ras. Blood **84:**3435–3459.
21. **Largaespada, D. A., J. D. Shaughnessy, N. A. Jenkins, and N. G. Copeland.** 1995. Retroviral insertion at the *Evi-2* locus in BXH-2 myeloid leukemia cell lines disrupts *Nf1* expression without changes in steady-state Ras-GTP levels. J. Virol. **69:**5095–5102.
22. **Largaespada, D. L., C. I. Brannan, N. A. Jenkins, and N. G. Copeland.** 1996. *Nf1* deficiency causes Ras-mediated granulocyte/macrophage stimulating factor hypersensitivity and chronic myeloid leukemia. Nat. Genet. **12:**137–143.
23. **Li, J., H. Shen, K. L. Himmel, A. J. Dupuy, D. L. Largaespada, T. Nakamura, J. D. J. Shaughnessy, N. A. Jenkins, and N. G. Copeland.** 1999. Leukemia disease genes: large-scale cloning and pathway predictions. Nat. Genet. **23:**348–353.
24. **McClinton, D., J. Stafford, L. Brents, T. P. Bender, and W. M. Kuehl.** 1990. Differentiation of mouse erythroleukemia cells is blocked by late up-regulation of a c-*myb* transgene. Mol. Cell. Biol. **10:**705–710.
25. **Moscow, J. J., F. Bullrich, K. Huebner, I. O. Daar, and A. M. Buchberg.** 1995. *Meis1*, a *PBX1*-related homeobox gene involved in myeloid leukemia in BXH-2 mice. Mol. Cell. Biol. **15:**5434–5443.
26. **Nakamura, T., D. A. Largaespada, J. D. Shaughnessy, N. A. Jenkins, and N. G. Copeland.** 1996. Cooperative activation of Hoxa and Pbx1-related genes in murine myeloid leukemias. Nat. Genet. **12:**149–153.
27. **Oh, I.-H., and E. P. Reddy.** 1999. The *myb* gene family in cell growth, differentiation and apoptosis. Oncogene **18:**3017–3033.
28. **Perkins, A. S.** 1989. The pathology of murine myelogenous leukemias. Curr. Top. Microbiol. Immunol. **149:**3–21.
29. **Robb, L., L. Mifsud, L. Hartley, C. Biben, N. G. Copeland, D. J. Gilbert, N. A. Jenkins, and R. P. Harvey.** 1998. Epicardin: a novel basic helix-loop-helix transcription factor gene expressed in epicardium, branchial arch myoblasts, and mesenchyme of developing lung, gut, kidney, and gonads. Dev. Dyn. **213:**105–113.
30. **Selvakumaran, M., D. A. Liebermann, and B. Hoffman-Liebermann.** 1992. Deregulated c-*myb* disrupts interleukin-6- or leukemia inhibitory factor-induced myeloid differentiation prior to c-*myc*: role in leukemogenesis. Mol. Cell. Biol. **12:**2493–2500.
31. **Shannon, K. M., P. O'Connell, G. A. Martin, D. Paderanga, K. Olson, P. Dinndorf, and F. McCormick.** 1994. Loss of the normal NF1 allele from the bone marrow of children with type 1 neurofibromatosis and malignant myeloid disorders. N. Engl. J. Med. **330:**597–601.
32. **Shannon, K. M., J. Watterson, P. Johnson, P. O'Connell, B. Lange, N. Shah, P. Steinherz, Y. W. Kan, and J. R. Priest.** 1992. Monosomy 7 myeloproliferative disease in children with neurofibromatosis, type 1: epidemiology and molecular analysis. Blood **79:**1311–1318.
33. **Side, L. E., P. D. Emanuel, B. Taylor, J. Franklin, P. Thompson, R. P. Castleberry, and K. M. Shannon.** 1998. Mutations of the *NF1* gene in children with juvenile myelomonocytic leukemia without clinical evidence of neurofibromatosis, type 1. Blood **92:**267–272.
34. **Stiller, C. A., J. M. Chessells, and M. Fitchett.** 1994. Neurofibromatosis and childhood leukaemia/lymphoma: a population-based UKCCSG study. Br. J. Cancer **70:**969–972.
35. **Todokoro, K., R. J. Watson, H. Higo, H. Amanuma, S. Kuramochi, H. Yanagisawa, and Y. Ikawa.** 1988. Down-regulation of c-*myb* gene expression is a prerequisite for erythropoietin-induced erythroid differentiation. Proc. Natl. Acad. Sci. USA **85:**8900–8904.
36. **Wolff, L.** 1996. Myb-induced transformation. Crit. Rev. Oncog. **7:**245–260.
37. **Yanagisawa, H., T. Nagasawa, S. Kuramochi, T. Abe, Y. Ikawa, and K. Todokoro.** 1991. Constitutive expression of exogenous c-*myb* gene causes maturation block in monocyte-macrophage differentiation. Biochim. Biophys. Acta **1088:**380–384.